EUROPEAN ORGANIZATION FOR NUCLEAR RESEARCH

A comparison of b and uds quark jets to gluon jets

The OPAL Collaboration

Abstract

Symmetric three-jet events are selected from hadronic Z^0 decays such that the two lower energy jets are each produced at an angle of about 150° with respect to the highest energy jet. In some cases, a displaced secondary vertex is reconstructed in one of the two lower energy jets, which permits the other lower energy jet to be identified as a gluon jet through anti-tagging. In other cases, the highest energy jet is tagged as a b jet or as a light quark (uds) jet using secondary vertex or track impact parameter and momentum information. Comparing the two lower energy jets of the events with a tag in the highest energy jet to the anti-tagged gluon jets yields a direct comparison of b, uds and gluon jets, which are produced with the same energy of about 24 GeV and under the same conditions. We observe b jets and gluon jets to have similar properties as measured by the angular distribution of particle energy around the jet directions and by the fragmentation functions. In contrast, gluon jets are found to be significantly broader and to have a markedly softer fragmentation function than uds jets. For the $k_\perp$ jet finder, we find

$$\frac{\langle n^{\text{ch.}} \rangle_{\text{gluon}}}{\langle n^{\text{ch.}} \rangle_{\text{b quark}}} = 1.089 \pm 0.024\,(\text{stat.}) \pm 0.024\,(\text{syst.})$$

$$\frac{\langle n^{\text{ch.}} \rangle_{\text{gluon}}}{\langle n^{\text{ch.}} \rangle_{\text{uds quark}}} = 1.390 \pm 0.038\,(\text{stat.}) \pm 0.032\,(\text{syst.})$$

as the ratios of the mean charged particle multiplicity in the gluon jets compared to the b and uds jets. Results are also reported using the cone jet finder.

(To be submitted to Zeitschrift für Physik C)

The OPAL Collaboration

G. Alexander[23], J. Allison[16], N. Altekamp[5], K. Ametewee[25], K.J. Anderson[9], S. Anderson[12], S. Arcelli[2], S. Asai[24], D. Axen[29], G. Azuelos[18,a], A.H. Ball[17], E. Barberio[26], R.J. Barlow[16], R. Bartoldus[3], J.R. Batley[5], G. Beaudoin[18], J. Bechtluft[14], A. Beck[23], G.A. Beck[13], C. Beeston[16], T. Behnke[8], K.W. Bell[20], G. Bella[23], S. Bentvelsen[8], P. Berlich[10], S. Bethke[14], O. Biebel[14], I.J. Bloodworth[1], P. Bock[11], H.M. Bosch[11], M. Boutemeur[18], S. Braibant[12], P. Bright-Thomas[25], R.M. Brown[20], H.J. Burckhart[8], C. Burgard[27], R. Bürgin[10], P. Capiluppi[2], R.K. Carnegie[6], A.A. Carter[13], J.R. Carter[5], C.Y. Chang[17], C. Charlesworth[6], D.G. Charlton[1,b], S.L. Chu[4], P.E.L. Clarke[15], J.C. Clayton[1], S.G. Clowes[16], I. Cohen[23], J.E. Conboy[15], O.C. Cooke[16], M. Cuffiani[2], S. Dado[22], C. Dallapiccola[17], G.M. Dallavalle[2], C. Darling[31], S. De Jong[12], L.A. del Pozo[8], H. Deng[17], M.S. Dixit[7], E. do Couto e Silva[12], E. Duchovni[26], G. Duckeck[8], I.P. Duerdoth[16], U.C. Dunwoody[8], J.E.G. Edwards[16], P.G. Estabrooks[6], H.G. Evans[9], F. Fabbri[2], B. Fabbro[21], P. Fath[11], F. Fiedler[12], M. Fierro[2], M. Fincke-Keeler[28], H.M. Fischer[3], R. Folman[26], D.G. Fong[17], M. Foucher[17], H. Fukui[24], A. Fürtjes[8], P. Gagnon[6], A. Gaidot[21], J.W. Gary[4], J. Gascon[18], S.M. Gascon-Shotkin[17], N.I. Geddes[20], C. Geich-Gimbel[3], S.W. Gensler[9], F.X. Gentit[21], T. Geralis[20], G. Giacomelli[2], P. Giacomelli[4], R. Giacomelli[2], V. Gibson[5], W.R. Gibson[13], J.D. Gillies[20], D.M. Gingrich[30,a], J. Goldberg[22], M.J. Goodrick[5], W. Gorn[4], C. Grandi[2], E. Gross[26], C. Hajdu[32], G.G. Hanson[12], M. Hansroul[8], M. Hapke[13], C.K. Hargrove[7], P.A. Hart[9], C. Hartmann[3], M. Hauschild[8], C.M. Hawkes[8], R. Hawkings[8], R.J. Hemingway[6], G. Herten[10], R.D. Heuer[8], J.C. Hill[5], S.J. Hillier[8], T. Hilse[10], P.R. Hobson[25], D. Hochman[26], R.J. Homer[1], A.K. Honma[28,a], D. Horváth[32,c], R. Howard[29], R.E. Hughes-Jones[16], D.E. Hutchcroft[5], P. Igo-Kemenes[11], D.C. Imrie[25], A. Jawahery[17], P.W. Jeffreys[20], H. Jeremie[18], M. Jimack[1], A. Joly[18], M. Jones[6], R.W.L. Jones[8], U. Jost[11], P. Jovanovic[1], J. Kanzaki[24], D. Karlen[6], K. Kawagoe[24], T. Kawamoto[24], R.K. Keeler[28], R.G. Kellogg[17], B.W. Kennedy[20], B.J. King[8], J. King[13], J. Kirk[29], S. Kluth[5], T. Kobayashi[24], M. Kobel[10], D.S. Koetke[6], T.P. Kokott[3], S. Komamiya[24], R. Kowalewski[8], T. Kress[11], P. Krieger[6], J. von Krogh[11], P. Kyberd[13], G.D. Lafferty[16], H. Lafoux[21], R. Lahmann[17], W.P. Lai[19], D. Lanske[14], J. Lauber[15], J.G. Layter[4], A.M. Lee[31], E. Lefebvre[18], D. Lellouch[26], J. Letts[2], L. Levinson[26], C. Lewis[15], S.L. Lloyd[13], F.K. Loebinger[16], G.D. Long[17], B. Lorazo[18], M.J. Losty[7], J. Ludwig[10], A. Luig[10], A. Malik[21], M. Mannelli[8], S. Marcellini[2], C. Markus[3], A.J. Martin[13], J.P. Martin[18], G. Martinez[17], T. Mashimo[24], W. Matthews[25], P. Mättig[3], J. McKenna[29], E.A. Mckigney[15], T.J. McMahon[1], A.I. McNab[13], F. Meijers[8], S. Menke[3], F.S. Merritt[9], H. Mes[7], J. Meyer[27], A. Michelini[8], G. Mikenberg[26], D.J. Miller[15], R. Mir[26], W. Mohr[10], A. Montanari[2], T. Mori[24], M. Morii[24], U. Müller[3], B. Nellen[3], B. Nijjhar[16], S.W. O'Neale[1], F.G. Oakham[7], F. Odorici[2], H.O. Ogren[12], N.J. Oldershaw[16], C.J. Oram[28,a], M.J. Oreglia[9], S. Orito[24], M. Palazzo[2], J. Pálinkás[33], J.P. Pansart[21], J.R. Pater[16], G.N. Patrick[20], M.J. Pearce[1], P.D. Phillips[16], J.E. Pilcher[9], J. Pinfold[30], D.E. Plane[8], P. Poffenberger[28], B. Poli[2], A. Posthaus[3], T.W. Pritchard[13], H. Przysiezniak[30], D.L. Rees[1], D. Rigby[1], M.G. Rison[5], S.A. Robins[13], N. Rodning[30], J.M. Roney[28], E. Ros[8], A.M. Rossi[2], M. Rosvick[28], P. Routenburg[30], Y. Rozen[8], K. Runge[10], O. Runolfsson[8], D.R. Rust[12], R. Rylko[25], M. Sasaki[24], C. Sbarra[2], A.D. Schaile[8], O. Schaile[10], F. Scharf[3], P. Scharff-Hansen[8], P. Schenk[4], B. Schmitt[3], M. Schröder[8], H.C. Schultz-Coulon[10], M. Schulz[8], P. Schütz[3], J. Schwiening[3], W.G. Scott[20], M. Settles[12], T.G. Shears[16], B.C. Shen[4], C.H. Shepherd-Themistocleous[7], P. Sherwood[15], G.P. Siroli[2], A. Sittler[27], A. Skillman[15], A. Skuja[17], A.M. Smith[8], T.J. Smith[28], G.A. Snow[17], R. Sobie[28], S. Söldner-Rembold[10], R.W. Springer[30], M. Sproston[20], A. Stahl[3], M. Starks[12], C. Stegmann[10], K. Stephens[16], J. Steuerer[28], B. Stockhausen[3], D. Strom[19], F. Strumia[8], P. Szymanski[20], R. Tafirout[18], P. Taras[18], S. Tarem[26], M. Tecchio[8], N. Tesch[3], M.A. Thomson[8], E. von Törne[3], S. Towers[6], M. Tscheulin[10], T. Tsukamoto[24], E. Tsur[23], A.S. Turcot[9], M.F. Turner-Watson[8], P. Utzat[11], R. Van Kooten[12], G. Vasseur[21], P. Vikas[18], M. Vincter[28], E.H. Vokurka[16], F. Wäckerle[10], A. Wagner[27], D.L. Wagner[9], C.P. Ward[5], D.R. Ward[5], J.J. Ward[15], P.M. Watkins[1], A.T. Watson[1], N.K. Watson[7], P. Weber[6], P.S. Wells[8], N. Wermes[3], B. Wilkens[10], G.W. Wilson[27], J.A. Wilson[1], T. Wlodek[26], G. Wolf[26], S. Wotton[11], T.R. Wyatt[16], S. Xella[2], G. Yekutieli[26], V. Zacek[18]

[1]School of Physics and Space Research, University of Birmingham, Birmingham B15 2TT, UK
[2]Dipartimento di Fisica dell' Università di Bologna and INFN, I-40126 Bologna, Italy
[3]Physikalisches Institut, Universität Bonn, D-53115 Bonn, Germany
[4]Department of Physics, University of California, Riverside CA 92521, USA
[5]Cavendish Laboratory, Cambridge CB3 0HE, UK
[6] Ottawa-Carleton Institute for Physics, Department of Physics, Carleton University, Ottawa, Ontario K1S 5B6, Canada
[7]Centre for Research in Particle Physics, Carleton University, Ottawa, Ontario K1S 5B6, Canada
[8]CERN, European Organization for Particle Physics, CH-1211 Geneva 23, Switzerland
[9]Enrico Fermi Institute and Department of Physics, University of Chicago, Chicago IL 60637, USA
[10]Fakultät für Physik, Albert Ludwigs Universität, D-79104 Freiburg, Germany
[11]Physikalisches Institut, Universität Heidelberg, D-69120 Heidelberg, Germany
[12]Indiana University, Department of Physics, Swain Hall West 117, Bloomington IN 47405, USA
[13]Queen Mary and Westfield College, University of London, London E1 4NS, UK
[14]Technische Hochschule Aachen, III Physikalisches Institut, Sommerfeldstrasse 26-28, D-52056 Aachen, Germany
[15]University College London, London WC1E 6BT, UK
[16]Department of Physics, Schuster Laboratory, The University, Manchester M13 9PL, UK
[17]Department of Physics, University of Maryland, College Park, MD 20742, USA
[18]Laboratoire de Physique Nucléaire, Université de Montréal, Montréal, Quebec H3C 3J7, Canada
[19]University of Oregon, Department of Physics, Eugene OR 97403, USA
[20]Rutherford Appleton Laboratory, Chilton, Didcot, Oxfordshire OX11 0QX, UK
[21]CEA, DAPNIA/SPP, CE-Saclay, F-91191 Gif-sur-Yvette, France
[22]Department of Physics, Technion-Israel Institute of Technology, Haifa 32000, Israel
[23]Department of Physics and Astronomy, Tel Aviv University, Tel Aviv 69978, Israel
[24]International Centre for Elementary Particle Physics and Department of Physics, University of Tokyo, Tokyo 113, and Kobe University, Kobe 657, Japan
[25]Brunel University, Uxbridge, Middlesex UB8 3PH, UK
[26]Particle Physics Department, Weizmann Institute of Science, Rehovot 76100, Israel
[27]Universität Hamburg/DESY, II Institut für Experimental Physik, Notkestrasse 85, D-22607 Hamburg, Germany
[28]University of Victoria, Department of Physics, P O Box 3055, Victoria BC V8W 3P6, Canada
[29]University of British Columbia, Department of Physics, Vancouver BC V6T 1Z1, Canada
[30]University of Alberta, Department of Physics, Edmonton AB T6G 2J1, Canada
[31]Duke University, Department of Physics, Durham, NC 27708-0305, USA
[32]Research Institute for Particle and Nuclear Physics, H-1525 Budapest, P O Box 49, Hungary
[33]Institute of Nuclear Research, H-4001 Debrecen, P O Box 51, Hungary

[a]Also at TRIUMF, Vancouver, Canada V6T 2A3
[b] Royal Society University Research Fellow
[c] Institute of Nuclear Research, Debrecen, Hungary

1   Introduction

Quantum Chromodynamics (QCD) predicts differences between the properties of jets initiated by gluons and those initiated by quarks. These differences are due to the different quark-gluon and gluon-gluon coupling strengths. In several earlier publications [1]-[3], we presented measurements of differences between quark- and gluon-initiated jets. Three jet events from hadronic Z^0 decays were selected such that the two lower energy jets, one of which was assumed to be a quark jet and the other a gluon jet, were both produced at an angle of about 150° with respect to the highest energy jet. In some cases, one of the two lower energy jets could be identified as a quark jet due to the presence of a displaced secondary vertex. The lower energy jet without the displaced secondary vertex was thereby identified as a gluon jet by anti-tagging. The properties of these anti-tagged gluon jets were compared to those of the two lower energy jets from the inclusive symmetric sample. The jets being compared thus had the same energy and were produced with the same topology relative to the other jets, leading to model independent results. An algebraic correction procedure was applied to obtain measurements corresponding to pure quark and gluon jets. It was observed that gluon jets were broader, had a softer fragmentation function, and a larger mean particle multiplicity than quark jets, in agreement with predictions from QCD models.

For these earlier studies, the flavor composition of the quark jet sample was governed by the Z^0 coupling strength to the individual flavors in the inclusive symmetric events. As a consequence, the five flavor types d, u, s, c and b were about equally represented.[1] It is also of interest to study quark and gluon jet properties and differences using quark jets with a specific flavor content. For example, theoretical calculations in QCD often assume zero quark masses. It is therefore relevant to select a light quark (uds) sample to compare to gluon jets, to facilitate comparison of data to analytic results. At the Tevatron collider at Fermilab, the t quark has been observed through its decay to b quarks [4]. A comparison of b quark jets to gluon jets is thus also of interest, to establish whether general jet properties can help to distinguish t quark events containing b jets from QCD background events containing gluon jets.

A study of b and light quark jets in comparison to gluon jets can easily be performed using our established analysis method by tagging the flavor of the highest energy jets in the inclusive symmetric sample. By requiring the highest energy jet to be a b jet, for example, the lower energy quark jet is forced to be a b jet even though no tagging conditions are imposed on it, and similarly for uds quark jets. Thus the two lower energy jets of the symmetric samples can be forced to be about 50% b or uds quark jets and 50% gluon jets without introducing large biases. These data may be compared to the anti-tagged gluon jet data obtained as in our earlier studies to extract a b or uds quark jet comparison to gluon jets.

In this paper, we present such a study of b, uds, and gluon jet properties. The data were collected with the OPAL detector at the e^+e^- collider LEP at CERN. In section 2, we provide a brief description of the OPAL detector and of the particle and event selection. Details of the analysis are given in section 3. The results are presented in section 4. Section 5 contains a summary and discussion.

---

[1]The quark flavor composition was estimated to be about 22% d and s quarks, 21% b quarks, and 17.5% u and c quarks.

2 Detector and data sample

The OPAL detector is described in detail elsewhere [5]. The tracking system consists of a silicon microvertex detector [6], an inner vertex chamber, a large volume jet chamber and specialized chambers at the outer radius of the jet chamber which improve the measurements in the z-direction.[2] The tracking system covers the region $|\cos\theta| < 0.95$ and is enclosed by a solenoidal magnet coil with an axial field of 0.435 T. Electromagnetic energy is measured by a lead-glass calorimeter located outside the magnet coil, which covers $|\cos\theta| < 0.98$.

The present analysis is based on a sample of about 2 800 000 hadronic events collected at e^+e^- center-of-mass energies within 250 MeV of the Z^0 peak by the OPAL detector from 1991 to 1994. The procedures for identifying hadronic events are discussed in [7]. Charged tracks and electromagnetic clusters were selected for the analysis as follows.[3] Charged tracks were required to have at least 20 measured points (of 159 possible) in the jet chamber, to have a momentum greater than 0.10 GeV/c, to lie in the region $|\cos\theta| < 0.94$ and to point to the origin to within 5 cm in the r-ϕ plane. In addition, they were required to yield a χ^2 per degree-of-freedom of less than 100 for the track fit in the r-ϕ plane. Clusters were required to be spread over at least two lead glass blocks and to have an energy greater than 0.10 GeV if they were in the barrel section of the detector ($|\cos\theta| < 0.82$) or greater than 0.30 GeV if they were in the endcap section ($0.82 < |\cos\theta| < 0.98$). To minimize double counting of energy, clusters were used only if they were not associated with a charged track. A cluster was associated with a charged track if the extrapolated track coordinates at the entrance to the calorimeter matched the cluster's position to better than 80 mrad in ϕ and 150 mrad in θ, if the cluster was in the barrel, or 50 mrad in both ϕ and θ, if it was in the endcap. Each accepted track and unassociated cluster was considered to be a particle. Tracks were assigned the pion mass. Clusters were assigned zero mass since they originate mostly from photons. Event cuts were applied to eliminate residual background and events in which a significant number of particles were lost near the beam direction. First, the number of accepted charged tracks was required to be at least five. Second, the thrust axis of the event was calculated using the particles and was required to satisfy $|\cos(\theta_{\text{thrust}})| < 0.9$. The residual background from all sources was estimated to be less than 1%.

3 Analysis procedure

3.1 Selection of three jet events

Three jet events are selected using two different jet finding methods: the $k_\perp$ [8] and cone [9, 10] methods. A detailed description of these algorithms is given in [3]. Use of these two jet finding methods permits us to assess the extent to which our conclusions depend on the jet definition.

---

[2] Our coordinate system is defined so that z is the coordinate parallel to the e^- beam axis, r is the coordinate normal to the beam axis, ϕ is the azimuthal angle around the beam axis and θ is the polar angle with respect to z.

[3] These criteria are identical to those chosen for our earlier work [2, 3] except that we accept tracks with momentum values down to 0.10 GeV/c, rather than with transverse momentum values $p_\perp$ down to 0.15 GeV/c, in order to reduce the size of the detector corrections in the lowest bin of the fragmentation functions (section 4).

The $k_\perp$ algorithm is a common one for the analysis of e$^+$e$^-$ annihilation data. It employs a single resolution parameter, y_{cut}. The cone algorithm is the usual choice for experiments at p$\overline{\text{p}}$ colliders. Use of the cone algorithm is therefore expected to facilitate the comparison of our data with jet data from p$\overline{\text{p}}$ experiments. The cone algorithm employs two resolution parameters: the cone size R and the minimum particle energy within the cone, ϵ. We use the same values for the jet resolution parameters that were chosen for our earlier studies [2, 3], namely y_{cut}=0.02, R=30° and ϵ=10 GeV. With the $k_\perp$ jet finder, all particles in an event are associated with a jet. Particles are not necessarily assigned to the jet to which they are nearest in angle. With the cone jet finder, soft particles between jets often lie outside the cones and are not assigned to any jet; those particles associated with a jet are always assigned to the jet to which they are nearest in angle.

Events reconstructed with exactly three jets, using either the $k_\perp$ or cone method, are retained for further study. These events are interpreted as arising from two quark jets and a gluon jet. Each jet is required to contain at least two particles and to lie in the polar angle region $|\cos\theta| < 0.9$. The sum of the angles between the three jets is required to exceed 358° to eliminate non-planar events. The jets in each event are assigned a calculated energy based on the angles between them, assuming massless kinematics and perfect event reconstruction. In the present study, jet energies refer to these calculated energies unless otherwise stated. Symmetric three jet events are selected by projecting the jets into the three jet event plane and requiring the angles between the jet with the highest energy and each of the two others to be 150 ± 10°. The event plane is defined by the plane normal to the smallest sphericity eigenvector. In total, 65 253 symmetric three jet events are found using the $k_\perp$ jet finder, and 51 452 using the cone jet finder. We refer to these events as the "normal-mixture" samples. About 65% of the normal-mixture events found using the cone algorithm are also found using the $k_\perp$ one. For the $k_\perp$ jet finder, the mean jet energies are 42.43 ± 0.01 GeV for the highest energy jet and 24.38 ± 0.01 GeV for the two lower energy jets. Essentially identical results are obtained using the cone jet finder. Since the highest energy jets have a much larger energy than the two lower energy ones, they are likely to be quark jets with high probability, due to the nature of the gluon radiation spectrum. From Monte Carlo study, this probability is estimated to be about 97%.

3.2   Selection of gluon jets

The method we introduced [2] for obtaining quark and gluon jet properties is based on the reconstruction of a displaced secondary vertex in one of the two lower energy jets of the normal-mixture events.[4] The secondary vertex is associated with heavy quark decay, especially that of the b quark. At LEP, b quarks are produced almost exclusively at the electro-weak vertex: thus a jet containing a b hadron is almost always a quark jet. The lower energy jets without secondary vertices thus constitute a highly enriched sample of anti-tagged gluon jets. To identify secondary vertices in jets, we employ the method given in [3]. Briefly, a secondary vertex is required to contain at least three tracks, two of which are "significant". A track is significant if its signed impact parameter value in the r-ϕ plane with respect to the primary event vertex,[5]

---

[4]Our original studies [1] were based on lepton tagging rather than secondary vertex tagging, but otherwise employed the same method.

[5]The method used to determine the primary event vertex position is presented in [11].

5

b, satisfies $b/\sigma_b > 2.5$, with σ_b the error of b. For jets with such a secondary vertex, the signed decay length, L, is calculated with respect to the primary vertex, along with its error, σ_L. To identify gluon jets, we require one of the lower energy jets in the normal-mixture events to contain a reconstructed secondary vertex with decay length significance, defined by L/σ_L, greater than 5.0, and the other lower energy jet not to contain a secondary vertex with L/σ_L greater than 2.0. We further require that the decay length L of the secondary vertex in the tagged jet be less than 0.6 cm. In total, 2 428 anti-tagged gluon jets are obtained using the $k_\perp$ jet finder and 2 072 jets using the cone one: we refer to these as the "gluon-tagged" jets. About 55% of the gluon-tagged events found using the cone algorithm are also found using the $k_\perp$ algorithm. For the $k_\perp$ jet finder, the mean energy of the anti-tagged gluon jets is 23.59 ± 0.06 GeV. For the cone jet finder, the corresponding value is 23.58 ± 0.07 GeV.

The purity of the gluon-tagged jets is evaluated using Monte Carlo events which include simulation of the OPAL detector [12] and the same analysis procedures as the data. The Jetset parton shower model [13], version 7.3, with an implementation as presented in [2] is used. Jetset provides a good description of the relevant distributions, as discussed in [3]. Each simulated hadron jet is associated with an underlying quark or gluon jet. To perform this association, Monte Carlo events are examined at the parton level. The two hadron jets closest in angle to the directions of the primary quark and anti-quark which have evolved from the Z^0 decay are considered to be the quark jets; the remaining jet is identified as the gluon jet. Using this method, the estimated purity of the gluon-tagged jets is found to be $92.7 \pm 0.5\%$ using the $k_\perp$ jet finder and $92.8 \pm 0.5\%$ using the cone jet finder, where the uncertainties are statistical. The quark jet background of about 7% arises due to imperfect b quark jet identification and because the highest energy jet in an event is sometimes the gluon jet. The quark and gluon jet fractions of the gluon-tagged jets, including the flavor composition of the 7% quark jet component, are given in Table 1.

3.3   Selection of b quark jets

To obtain a b quark jet sample to compare to the gluon-tagged jets, b jet selection criteria are applied to the highest energy jets of the normal-mixture events. Displaced secondary vertices are reconstructed in the highest energy jets using the method discussed in [3]. These secondary vertices are required to have at least three tracks, at least two significant tracks (defined by $b/\sigma_b > 2.5$), a decay length significance L/σ_L larger than 5.0, and a decay length L less than 1.0 cm. These requirements are essentially the same as those applied to the lower energy jets in section 3.2 except that the maximum allowed value of L has been increased from 0.6 cm to 1.0 cm because of the larger energy of the jets being examined. In total, 3 004 events are selected using the $k_\perp$ jet finder and 3 037 events using the cone jet finder: we refer to these events as the "b-tagged" samples. About 52% of the b-tagged events selected using the cone jet finder are also selected using the $k_\perp$ jet finder. For the $k_\perp$ jet finder, 15% of the events in the b-tagged sample are in common with those in the gluon-tagged sample. The corresponding value for the cone jet finder is 16%. The mean energies of the two lower energy jets in the b-tagged samples are 24.39 ± 0.04 GeV and 24.40 ± 0.04 GeV for the $k_\perp$ and cone jet finders, respectively.

Fig. 1(a) shows the distribution of L/σ_L in the highest energy jets of the normal-mixture

events, with jets defined using the $k_\perp$ jet finder, after all the requirements given above to select the b-tagged events have been applied except for that on L/σ_L. The corresponding result for the cone jet finder is shown in Fig. 1(b). The distributions are peaked at L/σ_L values near 6.0 rather than near zero because two significant tracks are required to be present in the vertices. The histogram shows the prediction from Jetset. The overall description of the data by the Monte Carlo is seen to be good. The contributions to the Monte Carlo result from uds jets and c jets are shown by the shaded regions in Fig. 1. The unshaded region shows the contribution from b jets. The contribution from gluon jets is negligible. The distributions are seen to be dominated by b jets for L/σ_L values larger than 5.0.

The quark and gluon jet fractions and flavor composition of the quark jets for the two lower energy jets of the b-tagged samples, as determined using Jetset, are listed in Table 1. These jets are seen to be composed of about 50% quark jets and 50% gluon jets, as expected. About 92% of the lower energy quark jets are estimated to be b jets using either jet finding method.

3.4 Selection of uds quark jets

To obtain a light quark jet sample to compare to the gluon-tagged jets, uds jet selection criteria are applied to the normal-mixture events. The selection criteria are based on the signed impact parameter significance, b/σ_b, and the scaled energy value, $x = 2 \cdot E/E_{c.m.}$, of charged tracks in the highest energy jets of these events.

An algorithm is applied to identify charged tracks which are consistent with arising from photon conversions. Removing such tracks from consideration, the number of tracks in the highest energy jets which have $b/\sigma_b > 2.5$, $N_{\text{sig.}}^{\text{h.e.}}$, is determined. The distribution of $N_{\text{sig.}}^{\text{h.e.}}$ is shown in Figs. 2(a) and (b) for the $k_\perp$ and cone jet methods. Included in Fig. 2 is the prediction of Jetset, which is seen to provide a reasonable description of the measurements. The contributions to the Monte Carlo result from b jets, c jets, gluon jets and uds jets are also shown. To obtain an event sample with an enhanced light quark component, we select events for which $N_{\text{sig.}}^{\text{h.e.}}$ is zero, corresponding to the leftmost bin of Fig. 2(a) or (b). Jetset predicts the flavor composition of the lower energy quark jets to be about 7% b, 15% c and 78% uds, using either jet finder, after this selection requirement has been applied.

To further reduce the contamination from c and b events, we determine the maximum x value, x_{max}, of charged tracks in the highest energy jet of each of the selected events. Fig. 3 shows the distribution of x_{max} for the two different jet finding methods. The corresponding Jetset predictions are also shown. Again, the Monte Carlo is seen to provide a reasonable description of the measurements. Because b and c quarks are more massive than d, u and s quarks, the jets they initiate are less likely to contain a charged stable track with a large x value. Thus, events are retained only if $x_{\text{max}} > 0.45$.

In total, 1 777 events are selected using the $k_\perp$ jet finder and 1 486 events using the cone jet finder: we refer to these samples as the "uds-tagged" samples. About 63% of the uds-tagged events selected using the cone jet finder are also selected using the $k_\perp$ jet finder. About 1% of these events are in common with the events in the gluon-tagged samples, using either jet finder. The mean energies of the two lower energy jets in the uds-tagged samples are 24.36 ± 0.05 GeV and 24.36 ± 0.06 GeV for the $k_\perp$ and cone methods.

The estimated quark and gluon jet fractions and the quark flavor composition of the two lower energy jets in the uds-tagged samples are listed in Table 1. As in the case of the b-tagged samples, these jets are seen to be composed of about 50% quark and 50% gluon jets. The estimated uds purity of the lower energy quark jets is $89.6 \pm 0.7\%$ and $90.5 \pm 0.7\%$ for the $k_\perp$ and cone methods, respectively.

3.5   Correction method

To obtain distributions corresponding to pure quark and pure gluon jet states, we employ the algebraic correction method which we introduced in [2]. If $D_{\mathrm{g.tag}}(z_i)$ represents a distribution constructed from the gluon-tagged jets, with z_i the content of bin i, then

$$D_{\mathrm{g.tag}}(z_i) = (1 - q_{\mathrm{g.tag}}) \cdot G(z_i) \; + \; q_{\mathrm{g.tag}} \cdot Q_{\mathrm{g.tag}}(z_i) \quad , \tag{1}$$

where $G(z_i)$ and $Q_{\mathrm{g.tag}}(z_i)$ are the distributions for pure gluon and quark jet states, with $q_{\mathrm{g.tag}}$ the fraction of the jets which are quark jets. From Table 1, $q_{\mathrm{g.tag}}$ is estimated to be 0.073 using the $k_\perp$ jet finder and 0.072 using the cone jet finder. The total uncertainties of these values, including both statistical and systematic terms, are 0.016 and 0.025, respectively, where the systematic contributions are evaluated as in [3]. If $D_{\mathrm{b.tag}}(z_i)$ represents the same distribution constructed from the two lower energy jets of the b-tagged sample, then

$$D_{\mathrm{b.tag}}(z_i) = (1 - q_{\mathrm{b.tag}}) \cdot G(z_i) \; + \; q_{\mathrm{b.tag}} \cdot Q_{\mathrm{b.tag}}(z_i) \quad , \tag{2}$$

where $G(z_i)$ and $Q_{\mathrm{b.tag}}(z_i)$ are the gluon and quark jet states, with $q_{\mathrm{b.tag}} = 0.502$ and 0.501 the estimates from Table 1 for the two jet definitions. The total uncertainty for $q_{\mathrm{b.tag}}$ is 0.009 for either jet finder, where again the systematic terms are evaluated as in [3]. Assuming that $G(z_i)$ is the same in relations (1) and (2), and that $Q_{\mathrm{g.tag}}(z_i)$ and $Q_{\mathrm{b.tag}}(z_i)$ are the same, the two equations may be inverted for $G(z_i)$ and $Q_{\mathrm{b.tag}}(z_i)$. The first of these assumptions, that $G(z_i)$ is the same in relations (1) and (2), is motivated by our requirement that the gluon jets be selected under the same circumstances in all cases: they appear in the same kinematic configuration and are defined using the same track and jet finding criteria. Furthermore, the properties of hard, acollinear gluon jets do not depend on the event flavor according to QCD [14]. The second of these assumptions, that the quark jet distributions $Q_{\mathrm{g.tag}}(z_i)$ and $Q_{\mathrm{b.tag}}(z_i)$ are the same, is not entirely accurate. For example, it is seen from Table 1 that the estimated b jet component using the $k_\perp$ jet finder is 91.8% for $Q_{\mathrm{b.tag}}(z_i)$ and 55.0% for $Q_{\mathrm{g.tag}}(z_i)$. However, since the value of $q_{\mathrm{g.tag}}$ is small, the quark jet distribution which results from inverting relations (1) and (2) is dominated by the properties of $Q_{\mathrm{b.tag}}(z_i)$. Monte Carlo study shows that the differences between $Q_{\mathrm{g.tag}}(z_i)$ and $Q_{\mathrm{b.tag}}(z_i)$ do not introduce a measurable bias into the unfolded quark jet distribution compared to the results we would obtain were the two distributions the same, relative to the size of the statistical uncertainties. Since the Monte Carlo is expected to simulate the differences between $Q_{\mathrm{g.tag}}(z_i)$ and $Q_{\mathrm{b.tag}}(z_i)$ with sufficient accuracy, residual biases are in any case removed by the correction procedure for detector acceptance and resolution, described below.

Analogously, we construct the distribution $D_{\mathrm{uds.tag}}(z_i)$ from the two lower energy jets of the uds-tagged sample, which yields

$$D_{\mathrm{uds.tag}}(z_i) = (1 - q_{\mathrm{uds.tag}}) \cdot G(z_i) \; + \; q_{\mathrm{uds.tag}} \cdot Q_{\mathrm{uds.tag}}(z_i) \quad , \tag{3}$$

with $q_{\mathrm{uds.tag}} = 0.502$ and 0.503 the estimates of the quark jet fractions from Table 1 for the two jet finders. The total uncertainties for these values are 0.009 and 0.011, respectively, where the systematic terms are evaluated in the same manner as for $q_{\mathrm{b.tag}}$. Inverting relations (1) and (3) yields pure gluon and quark jet distributions $G(z_i)$ and $Q_{\mathrm{uds.tag}}(z_i)$ under the same assumptions as discussed above for the b- and gluon-tagged data.

A bin-by-bin correction is applied to the measured distributions of $G(z_i)$, $Q_{\mathrm{b.tag}}(z_i)$ and $Q_{\mathrm{uds.tag}}(z_i)$ to correct them for detector acceptance and resolution. Correction factors are derived from two different samples of Jetset 7.3 Monte Carlo events. One sample includes initial-state photon radiation, simulation of the OPAL detector and the same selection and analysis procedures as the data including the tagging conditions and algebraic procedures to obtain pure quark and gluon jet information. Good agreement is found between the distributions derived from this Monte Carlo sample and the measured ones for all variables studied. The second Monte Carlo sample does not include initial-state photon radiation or detector simulation and treats all charged and neutral particles with mean lifetimes greater than $3 \cdot 10^{-10}$ s as stable. The same three jet event selection criteria as described in section 3.1 are applied except that the jets are not required to satisfy $|\cos\theta| < 0.9$. The quark and gluon jets in this second sample are identified with Monte Carlo information using the method given in section 3.2. Multiplicative correction factors are obtained by taking the ratios of the distributions predicted by the second sample to those predicted by the first one on a bin-by-bin basis. For the analysis of b jets versus gluon jets, only b events are included in the second Monte Carlo sample discussed above. For the analysis of uds jets versus gluon jets, only uds events are included: the relative proportions of d, u and s quarks are given by the Z^0 coupling strengths. Beyond the correction for detector effects, the bin-by-bin factors therefore also correct for the estimated 8% non-b and 10% non-uds quark jet components of the b- and uds-tagged samples, respectively.

Besides the correction terms determined using Jetset 7.3, bin-by-bin corrections are also calculated using version 7.4 of the program with the parameter set given in Table 2. This parameter set results from a global fit to OPAL measurements of: event shape distributions such as thrust; the mean charged particle multiplicity in c and b events; the single particle inclusive momentum spectra for $\pi^{\pm}$, $K^{\pm}$, $p(\overline{p})$ and Λ; and to LEP measurements of the single particle inclusive production rates of 26 identified hadrons in hadronic Z^0 decays [15]. In particular, orbitally excited mesons (L=1), absent from our implementation of version 7.3, are present in that for version 7.4. Furthermore, the c hadron decay tables were updated to be consistent with the values published in [16], polarization effects were added in τ decays [17], and the B_s hadron production rate from b quarks was increased from 7.4% to 12.0% to be consistent with our measurements [18]. There are significant differences between the predictions of the two Jetset versions for some of the jet properties we study here. For example, the mean charged particle multiplicity of b jets defined using the $k_{\perp}$ algorithm is found to be 8.11 ± 0.01 using Jetset 7.3 and 8.87 ± 0.01 using Jetset 7.4. Also, the mean scaled energy value of b hadrons, $\langle x_E \rangle_{\mathrm{B}}$, decreases from 0.694 for version 7.3 to 0.683 for version 7.4.[6] The properties of c quark jets also differ significantly between the two Jetset versions. Despite these differences, the bin-by-bin factors obtained from the two program versions agree with each other to within the statistical uncertainties. The jet purity values derived from version 7.4 are similarly found to agree with those listed in Table 1 for version 7.3. Therefore, the bin-by-bin corrections we apply

---

[6]Subsequent to the generation of the Jetset 7.4 sample including detector simulation used for the present work, we adjusted the values of PARJ(54) and PARJ(55) given in Table 2 to be -0.031 and -0.0038, respectively, in order to obtain better agreement with our measured value of $\langle x_E \rangle_{\mathrm{B}}$=0.695 $\pm$ 0.097 [19].

9

to the data are obtained by taking the weighted mean of the bin-by-bin factors from the two program versions: as a consequence, the statistical fluctuations introduced by the correction procedure are reduced.

4   Results

In this section, we present the results of our comparison of b and uds jets to gluon jets. The data are compared to the predictions of the Jetset, Herwig [20], Ariadne [21] and Cojets [22] QCD parton shower models. For Jetset, we use version 7.4 with the parameter set given in Table 2, including the updated values for the parameters ϵ_c and ϵ_b listed in the bottom part of that table. The versions of Herwig and Ariadne we use are 5.8 and 4.06, respectively. The parameter set of Herwig was tuned by us in a similar manner to that described for Jetset 7.4 in section 3.5 and is given in Table 3. The parameter values of Ariadne were tuned by us to provide a good description of global event characteristics in Z^0 decays and are given in [23]. For Cojets, we examine the predictions of version 6.23 and use the default parameter set provided by the Monte Carlo author, which also yields a good description of the global characteristics of hadronic Z^0 decays. The Monte Carlo samples are generated in the same manner as the Jetset samples without detector simulation discussed in section 3.5.

4.1   Comparison of b jets with gluon jets

One of the features which we showed to differ between gluon and normal-mixture quark jets is their width, as measured by the angular distribution of jet energy with respect to the jet axis [1]-[3]. Fig. 4 shows the normalized distribution of the b quark and gluon jet energy around the jet axis, $(1/E^{\rm jet})\,{\rm d}E^{\rm jet}/{\rm d}\chi$, with jets defined using the $k_\perp$ jet finder; χ is the angle between a particle and the axis of the jet to which it is assigned. The bin-by-bin factors used to correct for detector acceptance and resolution and for the 8% misidentification of b jets are shown in the small figure above the data distributions. Comparing the b jet data, shown by the solid points, to the gluon jet data, shown by the open points, it is seen that there is only a relatively small difference between the widths of the two jet types: thus the b jets are similar to the gluon jets. This result is in contrast to that which we obtained by comparing gluon jets to normal-mixture quark jets, in which case the gluon jets were observed to be much broader than the quark jets. Included in Fig. 4 are the predictions of Jetset and Herwig, both of which describe the general features of the data. The ratio of the gluon to the b jet measurements is shown in Fig. 5. In Fig. 5, the predictions of Ariadne and Cojets are included as well. These last two models are also seen to describe the overall characteristics of the measurements.

The similarity of the b and gluon jet data shown in Figs. 4 and 5 suggests that it will be difficult to separate t quark events from QCD background events at the Tevatron collider using jet shape information. However, the jets studied at the Tevatron generally have a larger energy than those we study here. To assess the effect of the jet energy, we include in Fig. 5 the prediction of Jetset for 48 GeV jets, obtained by applying the event selection of the present study to Monte Carlo events generated at e^+e^- center-of-mass energies of 180 GeV. It is seen

that Jetset predicts a substantially larger difference between b and gluon jets for the larger jet energy.

For the cone jet finder, we characterize the width of a jet using its energy profile, $\psi_E(r/R)$ [24], defined for a jet of half angle R as the fraction of the jet energy contained within a smaller cone of half angle r which is coaxial with the jet. A related variable is the differential jet energy profile, $\phi_E(r/R)$, defined by:

$$\phi_E(r/R) \equiv \frac{\mathrm{d}\psi_E(r/R)}{\mathrm{d}(r/R)} \quad , \tag{4}$$

with $\mathrm{d}(r/R)$ the bin width. In comparing quark and gluon jets, $\phi_E(r/R)$ is preferable to $\psi_E(r/R)$ because the bin-to-bin contents are less correlated. In Figs. 6 and 7, we present our measurements of $\psi_E(r/R)$ and $\phi_E(r/R)$ for the b and gluon jets: as for $k_\perp$ analysis, relatively little difference is observed between the two jet types. The ratio of the gluon to b jet measurements for the $\phi_E(r/R)$ distribution is shown in Fig. 8. Figs. 6-8 include the results from the Monte Carlo models, which are again seen to be in general agreement with the data. In Fig. 8, we also show the prediction of Jetset for the 48 GeV jets, which yields the same conclusion as discussed above for Fig. 5.

A second feature which we showed to differ between gluon and normal-mixture quark jets is the inclusive distribution of particle energy in the jets, known as the fragmentation function. Fig. 9 shows the charged particle fragmentation function, $(1/N_{\mathrm{event}}) \, \mathrm{d}n_{\mathrm{ch.}}/\mathrm{d}x_E$, of the b and gluon jets defined using the $k_\perp$ jet finder, where $x_E = E/E^{\mathrm{jet}}$ is the scaled energy of a particle with respect to the energy of the jet to which it is assigned. The ratio of the gluon to b jet data is shown in Fig. 10. The corresponding results for the cone jet finder are presented in Figs. 11 and 12. From these figures, it is again seen that the properties of b and gluon jets do not differ much. Again, this is in contrast to our results based on the normal-mixture quark jet sample, in which case the fragmentation function of the gluon jets was found to be much softer than that of the quark jets.

A third feature which we observed to differ between gluon and normal-mixture quark jets is the mean charged particle multiplicity, $\langle n^{\mathrm{ch.}} \rangle$. Table 4 lists the measured values of $\langle n^{\mathrm{ch.}} \rangle$ for the gluon and b jets, $\langle n^{\mathrm{ch.}} \rangle_{\mathrm{gluon}}$ and $\langle n^{\mathrm{ch.}} \rangle_{\mathrm{b\,quark}}$, as well as their ratio, using the two jet definitions. The corresponding Monte Carlo results are also given. For the ratio values, we obtain $1.089 \pm 0.024\,(\mathrm{stat.}) \pm 0.024\,(\mathrm{syst.})$ for the $k_\perp$ jet finder and $0.917 \pm 0.021\,(\mathrm{stat.}) \pm 0.033\,(\mathrm{syst.})$ for the cone jet finder, where the systematic uncertainties are discussed in section 4.4. These ratios are considerably smaller than those we observed between gluon and normal-mixture quark jets, which were $1.251 \pm 0.024\,(\mathrm{stat.}) \pm 0.029\,(\mathrm{syst.})$ and $1.096 \pm 0.023\,(\mathrm{stat.}) \pm 0.023\,(\mathrm{syst.})$, respectively [3]. The difference between the results found using the $k_\perp$ and cone jet finders is due to the contributions of soft particles at relatively large angles to the jet axes, as discussed in [3].

4.2   Comparison of uds jets with gluon jets

In Figs. 13-17, we present our comparison of the uds and gluon jet widths. The $(1/E^{\mathrm{jet}}) \, \mathrm{d}E^{\mathrm{jet}}/\mathrm{d}\chi$ distributions and their ratio, defined using the $k_\perp$ algorithm, are shown in Figs. 13-14. The $\psi_E(r/R)$ and $\phi_E(r/R)$ distributions and the ratio of the $\phi_E(r/R)$ measurements, defined using

the cone jet finder, are shown in Figs. 15-17. Large differences are observed between the uds and gluon jets: the latter are seen to be much broader than the former. This result is not surprising, since large differences were also observed in our study of gluon and normal-mixture quark jets. Since the b jet component (about 21% of the normal-mixture quark jet sample) has been removed for the study presented in this section, and since b jets and gluon jets are observed to have similar widths (Figs. 4-8), it can be anticipated that the differences between uds and gluon jets will be large. The predictions of the Monte Carlo models, included in Figs. 13-17, are generally seen to be adequate.

Similarly, we present in Figs. 18-21 the uds and gluon jet fragmentation functions and their ratio for the two jet definitions. Again, large differences are observed between the uds and gluon jets: the gluon jet fragmentation function is seen to be much softer than that of the uds quarks. Again, this is not surprising, since a large difference was observed between the gluon and normal-mixture quark jet fragmentation functions in our earlier studies, and since the contributions of b quark jets, which exhibit little difference compared to gluon jets (Figs. 9-12), have been removed.

The mean charged particle multiplicity values of the uds and gluon jets, $\langle n^{\mathrm{ch.}} \rangle_{\mathrm{uds\,quark}}$ and $\langle n^{\mathrm{ch.}} \rangle_{\mathrm{gluon}}$, and the ratio between the two are presented in Table 5 along with the corresponding Monte Carlo results. For the $k_\perp$ and cone jet finders, we find $\langle n^{\mathrm{ch.}} \rangle_{\mathrm{gluon}}/\langle n^{\mathrm{ch.}} \rangle_{\mathrm{uds\,quark}}$ to be $1.390 \pm 0.038\,(\mathrm{stat.}) \pm 0.032\,(\mathrm{syst.})$ and $1.135 \pm 0.031\,(\mathrm{stat.}) \pm 0.029\,(\mathrm{syst.})$, respectively. These ratios are larger than those observed between gluon and normal-mixture quark jets in our earlier study [3], summarized at the end of section 4.1.

Comparing the value of $\langle n^{\mathrm{ch.}} \rangle_{\mathrm{gluon}}$ derived from the analysis of uds and gluon jets using the $k_\perp$ jet finder, given in Table 5, to the corresponding value derived from the analysis of b and gluon jets, given in Table 4, it is seen that essentially the same result is obtained: $\langle n^{\mathrm{ch.}} \rangle_{\mathrm{gluon}} = 9.16 \pm 0.14$ in the first case and $\langle n^{\mathrm{ch.}} \rangle_{\mathrm{gluon}} = 9.14 \pm 0.14$ in the second, where the statistical and systematic uncertainties have been combined in quadrature. For the cone jet finder, the value of $\langle n^{\mathrm{ch.}} \rangle_{\mathrm{gluon}}$ is found to be 6.18 ± 0.14 from the uds jet analysis and 6.13 ± 0.14 from the b jet analysis, which similarly agree with each other to within the experimental uncertainties. This agreement between the values of $\langle n^{\mathrm{ch.}} \rangle_{\mathrm{gluon}}$, despite the large differences in the quark jet properties $Q_{\mathrm{b.tag}}(z_i)$ and $Q_{\mathrm{uds.tag}}(z_i)$ in relations (2) and (3), illustrates the consistency of our analysis technique and results. From the Monte Carlo, for which the statistical errors are very small, it may be seen from Tables 4 and 5 that the predictions for $\langle n^{\mathrm{ch.}} \rangle_{\mathrm{gluon}}$ differ in some cases between the b and uds samples. For example, $\langle n^{\mathrm{ch.}} \rangle_{\mathrm{gluon}}$ is found to be 8.79 ± 0.01 for the b events and 8.62 ± 0.01 for the uds events using the Herwig generator with the $k_\perp$ definition. A similar difference is observed for Ariadne using this jet finder. This difference is not present for Jetset and Cojets or for any of the models using the cone jet finder, however. These differences for $\langle n^{\mathrm{ch.}} \rangle_{\mathrm{gluon}}$ observed using Herwig and Ariadne with the $k_\perp$ jet finder may nonetheless imply a small violation of our assumption that the gluon jet properties are independent of the event flavor. For example, b events have a larger overall particle multiplicity than uds events, which might result in differences in the manner in which tracks are assigned to the gluon jet by the jet finder for some of the models. The effect is more likely to be observed using the $k_\perp$ jet finder than the cone one since the $k_\perp$ algorithm allows particles very close to the quark jet axis to be assigned to the gluon jet. This effect – related to our reliance on a jet finding algorithm to assign particles to jets – results in only a relatively small ambiguity concerning the definition

of the jet properties and we do not consider it to represent a source of uncertainty for our measurements.

4.3 Comparison of the normal-mixture, b and uds quark jet data

It is also of interest to directly compare the results obtained for b and uds jets to each other and to the corresponding results derived using the normal-mixture events. In Figs. 22-26 this comparison is presented, for the $(1/E^{\mathrm{jet}})\,\mathrm{d}E^{\mathrm{jet}}/\mathrm{d}\chi$ and $(1/N_{\mathrm{event}})\,\mathrm{d}n_{\mathrm{ch.}}/\mathrm{d}x_E$ distributions defined using the $k_\perp$ jet finder (Figs. 22 and 23) and for the $\psi_{\mathrm{E}}(r/R)$, $\phi_{\mathrm{E}}(r/R)$ and $(1/N_{\mathrm{event}})\,\mathrm{d}n_{\mathrm{ch.}}/\mathrm{d}x_E$ distributions defined using the cone jet finder (Figs. 24-26). The solid points show the b jet data, the open points the uds jet data, and the shaded regions the normal-mixture quark jet data. The normal-mixture quark jet measurements were obtained as in our earlier publications [2, 3] but using the track selection of the present study: the results differ only slightly from those we presented previously. The experimental statistical uncertainties are shown. For the normal-mixture quark jet data, these uncertainties are indicated by the width of the shaded regions. The gluon jet distributions derived from the three analyses (b jet versus gluon jet, uds jet versus gluon jet and normal-mixture quark jet versus gluon jet) are virtually identical and are indicated by the dashed lines in Figs. 22-26. The uncertainties of the gluon jet data are of similar size to those shown for the normal-mixture quark jets.

Figs. 22-26 emphasize the results from sections 4.1 and 4.2: gluon jets are much broader and have a much softer fragmentation function than uds jets, while their properties are similar to b jets. The normal-mixture quark jet data are seen to lie between the uds and b jet measurements, as can be expected. From the Jetset Monte Carlo, we obtain the prediction that the properties of c quark jets also lie between those of b jets and uds jets, while being more similar to the latter than to the former.

4.4 Systematic uncertainties

To assess systematic uncertainties for the measurements presented in sections 4.1 and 4.2, the analysis was repeated with the following variations relative to the standard analysis.

1. Charged tracks alone were used for the Monte Carlo samples which include detector simulation and for the data, rather than charged tracks plus unassociated electromagnetic clusters.

2. The values of the algebraic correction coefficients $q_{\mathrm{g.tag}}$, $q_{\mathrm{b.tag}}$ and $q_{\mathrm{uds.tag}}$ were changed by their total uncertainties given in section 3.5 using the combination that resulted in the largest deviation with respect to the standard results.

3. Charged tracks were required to point to the event origin to within 2 cm in the r-ϕ plane, rather than 5 cm.

4. Charged tracks and electromagnetic clusters were restricted to the barrel region of the detector only, $|\cos(\theta_{\mathrm{particle}})| < 0.70$, rather than $|\cos(\theta_{\mathrm{particle}})| < 0.94$ for the charged tracks and $|\cos(\theta_{\mathrm{particle}})| < 0.98$ for the clusters.

13

5. A minimum of five particles was required to be present in each jet, rather than two.

6. The angle between the highest energy jet in an event and the two lower energy ones was required to be $150 \pm 5°$ rather than $150 \pm 10°$.

7. Herwig was used to estimate the quark jet purities, $q_{\text{g.tag}}$, $q_{\text{b.tag}}$ and $q_{\text{uds.tag}}$, and to determine the bin-by-bin correction factors, rather than Jetset.

8. The gluon jet selection described in section 3.2 was performed by reducing the number of tracks required to form a secondary vertex from three to two, and by requiring

   (a) one of the two lower energy jets in the normal-mixture samples to contain a reconstructed secondary vertex with a positive decay length L between 0.15 and 0.50 cm, with a decay length error σ_L less than 0.10 cm, and

   (b) the other lower energy jet not to have a secondary vertex or else to have a decay length less than 0.15 cm,

   which yields an estimated gluon jet purity of about 78%.

9. The b jet selection described in section 3.3 was performed by reducing the number of tracks required to form a secondary vertex from three to two, and by applying the criteria given in item 8(a) above to the highest energy jets, yielding an estimated purity of about 73% for the b component of the lower energy quark jets.

10. The uds jet selection described in section 3.4 was performed without the requirement on x_{max}, thus by using the b/σ_b values of tracks alone, resulting in an estimated purity of about 78% for the uds component of the lower energy quark jets.

For the cone jet finder, an additional check was made for the distributions based on energy measurements (the $\psi_{\text{E}}(r/R)$ and $\phi_{\text{E}}(r/R)$ distributions) by repeating the analysis using only electromagnetic calorimeter clusters for the Monte Carlo samples with detector simulation and for the data. For this analysis, all clusters – both those associated and those not associated with charged tracks – were used, and a requirement that at least eight clusters be present in an event replaced the requirement of at least five charged tracks. Secondary vertices were defined in the calorimeter-only case by using charged tracks which fell within the cones defined by the clusters. Similarly, charged tracks which fell within the cones of the highest energy jets were used to tag uds events in the manner described in section 3.4. A calorimeter-only analysis was not performed using the $k_\perp$ jet finder because it is not obvious how to assign charged tracks to the calorimeter-only jets, in order to tag the jets, in a manner that preserves the integrity of the jet definition.

Comparing the results obtained from these variations of the analysis to the standard results, systematic effects are observed only for the analysis based on charged tracks alone and for that in which the values of $q_{\text{g.tag}}$, $q_{\text{b.tag}}$ and $q_{\text{uds.tag}}$ are changed by their total uncertainties. For the analysis based on charged tracks alone, the gluon jet fragmentation function is found to be systematically softer than in the standard analysis for the studies presented both in sections 4.1 and 4.2 and for both jet definitions: no systematic trends are observed for the quark jet fragmentation functions or for any of the other distributions, however. In contrast, the results obtained using the other variations of the analysis, corresponding to items 3-10

14

in the above list, do not result in visible systematic deviations from the standard results for any of the distributions studied. Instead, bin-to-bin fluctuations above and below the standard results are observed, which are small compared to the statistical uncertainties and which exhibit no clear systematic trend. Therefore, for the distributions involving measurements of the jet width (the $(1/E^{\rm jet})\,{\rm d}E^{\rm jet}/{\rm d}\chi$, $\psi_{\rm E}(r/R)$ and $\phi_{\rm E}(r/R)$ distributions, and the corresponding ratios for the first and last of these) and for the b and uds quark jet fragmentation functions, two sources of systematic uncertainty are included: the difference between the standard results and those obtained using the extreme values of the algebraic correction coefficients, and the statistical uncertainty due to the detector correction factors. For the gluon jet fragmentation functions and mean charged particle multiplicity values, three sources of systematic uncertainty are included: the above two, plus the difference between the standard results and those found using the charged track measurements alone. The total uncertainties, given by the quadrature sum of the systematic and experimental statistical terms, are shown by the vertical error lines in Figs. 4-21. For each data point, the size of the experimental statistical error is indicated by the small horizontal bars. The systematic uncertainties for the mean multiplicity measurements are given in Tables 4 and 5. For the ratio of the gluon to quark jet multiplicities, an explicit breakdown of the contributions of the various systematic terms is given in Table 6.

5 Summary and conclusions

In this paper, we have extended our study of quark and gluon jet properties and differences by selecting quark jets with a specific flavor content, to obtain a comparison of b and light (uds) quark jets to gluon jets. As for our earlier studies, the quark and gluon jets being compared have essentially the same energy (about 24 GeV) and are produced under virtually identical conditions, leading to a direct and unambiguous interpretation of the results. The current study – emphasizing the quark flavor selection – complements our earlier work [3], in which the principal emphasis was on the jet definition.

We observe gluon jets and b jets to have similar properties, as measured by their broadness and fragmentation functions. The broadness of a jet is determined using its energy profile, namely the angular distribution of particle energy with respect to the jet axis normalized by the total jet energy. The ratio of the mean charged particle multiplicity between the two jet types is found to be $\langle n^{\rm ch.}\rangle_{\rm gluon}/\langle n^{\rm ch.}\rangle_{\rm b\,quark}= 1.089 \pm 0.024\,({\rm stat.}) \pm 0.024\,({\rm syst.})$ using the $k_\perp$ jet finder and $\langle n^{\rm ch.}\rangle_{\rm gluon}/\langle n^{\rm ch.}\rangle_{\rm b\,quark}= 0.917 \pm 0.021\,({\rm stat.}) \pm 0.033\,({\rm syst.})$ using the cone jet finder. These results suggest that it will be difficult to separate top quark events from QCD background events at the $p\overline{p}$ Tevatron collider using information based on internal jet shapes, for jet energies similar to ours. The Monte Carlo predicts substantially larger differences between b and gluon jets for jet energies of 48 GeV, compared to 24 GeV, however.

In contrast, gluon jets are found to be much broader and to have a much softer fragmentation function than uds jets. These results are consistent with those we obtained using normal-mixture quark jets for which d, u, s, c and b jets are present in about equal proportions [1]-[3]. The charged particle multiplicity ratio values obtained using the uds quark jet sample are $\langle n^{\rm ch.}\rangle_{\rm gluon}/\langle n^{\rm ch.}\rangle_{\rm uds\,quark}= 1.390 \pm 0.038\,({\rm stat.}) \pm 0.032\,({\rm syst.})$ and $1.135 \pm 0.031\,({\rm stat.}) \pm 0.029\,({\rm syst.})$ for the $k_\perp$ and cone jet finders. The quantitative differences observed between the two different jet definitions emphasize the need to employ methods which do not rely upon

the jet finder assignment of particles to jets, in order to obtain results which can be directly compared to analytic calculations [25].

6 Acknowledgements

References

[1] OPAL Collaboration, M.Z. Akrawy *et al.*, Phys. Lett. **B261** (1991) 334;
OPAL Collaboration, G. Alexander *et al.*, Phys. Lett. **B265** (1991) 462.

[2] OPAL Collaboration, P.D. Acton *et al.*, Z. Phys. **C58** (1993) 387.

[3] OPAL Collaboration, R. Akers *et al.*, "A model independent measurement of quark and gluon jet properties and differences", CERN-PPE/95-075, to appear in Z. Phys. **C**.

[4] CDF Collaboration, F. Abe *et al.*, Phys. Rev. Lett **74** (1995) 2626;
D0 Collaboration, S. Abachi *et al.* Phys. Rev. Lett **74** (1995) 2632.

[5] OPAL Collaboration, K. Ahmet *et al.*, Nucl. Instr. and Meth. **A305** (1991) 275.

[6] P. Allport *et al.*, Nucl. Instr. and Meth. **A324** (1993) 34;
P. Allport *et al.*, Nucl. Instr. and Meth. **A346** (1994) 476.

[7] OPAL Collaboration, G. Alexander *et al.*, Z. Phys. **C52** (1991) 175.

[8] S. Catani *et al.*, Phys. Lett. **B269** (1991) 432.

[9] J.E. Huth *et al.*, *Research Directions for the Decade*, Snowmass (1990), p.134, ed. E.L. Berger (World Scientific, Singapore);
CDF Collaboration, F. Abe *et al.*, Phys. Rev. **D45** (1992) 1448.

[10] OPAL Collaboration, R. Akers *et al.*, Z. Phys. **C63** (1994) 197.

[11] OPAL Collaboration, P.D. Acton *et al.*, Phys. Lett. **B273** (1991) 355.

[12] J. Allison *et al.*, Nucl. Instr. and Meth. **A317** (1992) 47.

[13] T. Sjöstrand, Comp. Phys. Comm. **39** (1986) 347;
T. Sjöstrand and M. Bengtsson, Comp. Phys. Comm. **43** (1987) 367;
T. Sjöstrand, CERN-TH.6488/92.

[14] V. Khoze in Proc. Int. Symp. Lepton Photon Interactions, Stanford 1989, ed. M. Riordan (World Scientific, Singapore) 1990.

[15] R. Hemingway in Proc. XXVII Int. Conf. on High Energy Physics, Glasgow 1994, ed. P.J. Bussey and I.G. Knowles (Institute of Physics Publishing, Bristol and Philadelphia);

[16] Review of Particle Properties, Phys. Rev. **D50** (1994) 1173.

[17] S. Jadach, Z. Was, R. Decker and J.H. Kühn, Comp. Phys. Comm. **76** (1993) 361.

[18] OPAL Collaboration, R. Akers *et al.*, Z. Phys. **C66** (1995) 555.

[19] OPAL Collaboration, R. Akers *et al.*, "A study of b quark fragmentation into B^0 and B^+ mesons at LEP", CERN-PPE/95-122, to appear in Phys. Lett. **B**.

[20] G. Marchesini, B.R. Webber *et al.*, Comp. Phys. Comm. **67** (1992) 465.

[21] L. Lönnblad, Comp. Phys. Comm. **71** (1992) 15.

17

[22] R. Odorico, Comp. Phys. Comm. **32** (1984) 139;
R. Odorico, Comp. Phys. Comm. **59** (1990) 527.

[23] OPAL Collaboration, M. Z. Akrawy *et al.*, Z. Phys. **C47** (1990) 505.

[24] CDF Collaboration, F. Abe *et al.*, Phys. Rev. Lett. **70** (1993) 713.

[25] J.W. Gary, Phys. Rev. **D49** (1994) 4503.

Sample	Gluon jet fraction	Quark jet fraction	Flavor mixture of the quark jet fraction				
			d	u	s	c	b
$k_\perp$ method:							
gluon-tagged	92.7 ± 0.5	7.3 ± 0.5	8.0 ± 1.9	6.5 ± 1.7	16.5 ± 2.6	14.0 ± 2.5	55.0 ± 3.5
b-tagged	49.8 ± 0.6	50.2 ± 0.6	0.8 ± 0.2	0.5 ± 0.1	0.8 ± 0.2	6.1 ± 0.4	91.8 ± 0.5
uds-tagged	49.8 ± 0.8	50.2 ± 0.8	31.1 ± 1.0	29.3 ± 1.0	29.3 ± 1.0	6.3 ± 0.5	4.0 ± 0.4
cone method:							
gluon-tagged	92.8 ± 0.5	7.2 ± 0.5	11.3 ± 2.4	8.3 ± 2.1	13.1 ± 2.6	16.7 ± 2.9	50.6 ± 3.9
b-tagged	49.9 ± 0.6	50.1 ± 0.6	0.6 ± 0.1	0.3 ± 0.1	0.5 ± 0.1	6.5 ± 0.4	92.1 ± 0.5
uds-tagged	49.7 ± 0.8	50.3 ± 0.8	31.5 ± 1.1	29.6 ± 1.1	29.4 ± 1.1	5.6 ± 0.5	3.9 ± 0.5

Table 1: Quark and gluon jet fractions measured in percent and flavor mixture of the quark jets for the lower energy jets of the symmetric events, as determined from the Jetset Monte Carlo, version 7.3, including simulation of the detector. The uncertainties are statistical.

Parameter	Monte Carlo Name	Default value	Optimized value
Peterson Option	MSTJ(11)	4	3
qq/q	PARJ(1)	0.100	0.085 ± 0.005
s/u	PARJ(2)	0.30	0.31 ± 0.01
(us/ud)·(u/s)	PARJ(3)	0.40	0.45 ± 0.04
V_{ud}	PARJ(4)	0.050	0.025 ± 0.005
$V_{d,u}$	PARJ(11)	0.50	0.60 ± 0.10
V_s	PARJ(12)	0.60	0.40 ± 0.05
$V_{c,b}$	PARJ(13)	0.75	0.72
Axial mesons (S=0,L=1)	PARJ(14)	0.00	0.43
Scalar mesons (S=1,L=1)	PARJ(15)	0.00	0.08
Axial mesons (S=1,L=1)	PARJ(16)	0.00	0.08
Tensor mesons (S=1,L=1)	PARJ(17)	0.00	0.17
σ_q	PARJ(21)	0.36	0.40 ± 0.03
a	PARJ(41)	0.30	0.11
b	PARJ(42)	0.58	0.52 ± 0.04
ϵ_c (old value)	PARJ(54)	-0.050	-0.046
ϵ_b (old value)	PARJ(55)	-0.0050	-0.0057
Λ_{LLA}	PARJ(81)	0.290	0.250 ± 0.006
Q_0	PARJ(82)	1.00	1.90 ± 0.50
ϵ_c (updated value)	PARJ(54)	-0.050	-0.031 ± 0.011
ϵ_b (updated value)	PARJ(55)	-0.0050	-0.0038 ± 0.0010

Table 2: Optimized OPAL parameter set for Jetset, version 7.4. Parameters not listed were left at their default values. The values of the parameters PARJ(13)-PARJ(17) were adjusted to describe single particle inclusive production rates at LEP, the parameters PARJ(41), PARJ(54) and PARJ(55) were taken from our previous parameter set for Jetset, and the other parameters listed were adjusted in a global fit. Uncertainties are given for the parameters employed in the fit. These uncertainties are the $\pm 1\sigma$ limits obtained from the χ^2 contours. Subsequent to the Monte Carlo generation with detector simulation used for the present work, the values of ϵ_c and ϵ_b were updated to those shown in the bottom part of the table in order to improve the description of our measured value for the mean scaled energy of b hadrons, $\langle x_E \rangle_B$.

Parameter	Monte Carlo Name	Default value	Optimized value
Λ_{MLLA}	QCDLAM	0.180	0.160 ± 0.005
Cluster mass parameter 1	CLMAX	3.35	3.40 ± 0.20
Cluster mass parameter 2	CLPOW	2.00	1.30
Gluon mass	RMASS(13)	0.75	0.75
Gluon virtuality cutoff	VGCUT	0.10	0.10
Quark virtuality cutoff	VQCUT	0.48	0.48
Smearing of cluster direction	CLSMR	0.00	$0.35^{+0.65}_{-0.05}$

Table 3: Optimized OPAL parameter set for Herwig, version 5.8, obtained in a global fit of the parameters listed. Parameters not listed were left at their default values. The uncertainties given for QCDLAM, CLMAX and CLSMR are the $\pm 1\sigma$ limits from the χ^2 contours. The other parameters do not exhibit clear minima in the χ^2 contours and no uncertainties are evaluated for them.

	$\langle n^{\text{ch.}} \rangle_{\text{gluon}}$	$\langle n^{\text{ch.}} \rangle_{\text{b quark}}$	$\langle n^{\text{ch.}} \rangle_{\text{gluon}} / \langle n^{\text{ch.}} \rangle_{\text{b quark}}$
$k_\perp$ method:			
OPAL data	$9.14 \pm 0.07 \pm 0.12$	$8.41 \pm 0.07 \pm 0.06$	$1.089 \pm 0.024 \pm 0.024$
	(1.024)	(0.933)	(1.099)
Jetset 7.4	9.30 ± 0.01	8.70 ± 0.01	1.069 ± 0.001
Herwig 5.8	8.79 ± 0.01	9.17 ± 0.01	0.959 ± 0.001
Ariadne 4.06	9.13 ± 0.01	8.69 ± 0.01	1.050 ± 0.001
Cojets 6.23	9.60 ± 0.01	8.90 ± 0.01	1.078 ± 0.002
48 GeV jets	12.61 ± 0.02	10.75 ± 0.02	1.173 ± 0.003
cone method:			
OPAL data	$6.13 \pm 0.06 \pm 0.13$	$6.68 \pm 0.05 \pm 0.09$	$0.917 \pm 0.021 \pm 0.033$
	(0.990)	(0.927)	(1.068)
Jetset 7.4	6.49 ± 0.01	6.82 ± 0.01	0.952 ± 0.001
Herwig 5.8	6.11 ± 0.01	7.10 ± 0.01	0.861 ± 0.002
Ariadne 4.06	6.08 ± 0.01	6.89 ± 0.01	0.882 ± 0.002
Cojets 6.23	6.24 ± 0.01	6.34 ± 0.01	0.984 ± 0.002
48 GeV jets	9.58 ± 0.02	8.97 ± 0.02	1.069 ± 0.003

Table 4: Mean charged particle multiplicity values of b jets and gluon jets. The numbers in parentheses are the bin-by-bin correction factors. The uncertainties given for the data include the experimental statistical (first error) and systematic (second error) terms. For the Monte Carlo results, the statistical uncertainties are given. The Jetset 7.4 prediction for 48 GeV jets, obtained by employing an e^+e^- center-of-mass energy of 180 GeV and the same event selection as applied to the other models, is also given.

	$\langle n^{\text{ch.}}\rangle_{\text{gluon}}$	$\langle n^{\text{ch.}}\rangle_{\text{uds quark}}$	$\langle n^{\text{ch.}}\rangle_{\text{gluon}}/\langle n^{\text{ch.}}\rangle_{\text{uds quark}}$
$k_\perp$ method:			
OPAL data	$9.16 \pm 0.07 \pm 0.12$	$6.59 \pm 0.06 \pm 0.10$	$1.390 \pm 0.038 \pm 0.032$
	(1.010)	(0.902)	(1.121)
Jetset 7.4	9.28 ± 0.01	6.58 ± 0.01	1.410 ± 0.002
Herwig 5.8	8.62 ± 0.01	6.29 ± 0.01	1.371 ± 0.002
Ariadne 4.06	9.01 ± 0.01	6.49 ± 0.01	1.389 ± 0.003
Cojets 6.23	9.62 ± 0.01	7.69 ± 0.01	1.251 ± 0.003
48 GeV jets	12.64 ± 0.02	8.79 ± 0.02	1.438 ± 0.004
cone method:			
OPAL data	$6.18 \pm 0.06 \pm 0.13$	$5.44 \pm 0.05 \pm 0.04$	$1.135 \pm 0.031 \pm 0.029$
	(0.984)	(0.893)	(1.101)
Jetset 7.4	6.52 ± 0.01	5.24 ± 0.01	1.245 ± 0.002
Herwig 5.8	6.07 ± 0.01	4.92 ± 0.01	1.233 ± 0.002
Ariadne 4.06	6.07 ± 0.01	5.16 ± 0.01	1.177 ± 0.003
Cojets 6.23	6.25 ± 0.01	5.38 ± 0.01	1.162 ± 0.003
48 GeV jets	9.63 ± 0.02	7.17 ± 0.02	1.343 ± 0.004

Table 5: Mean charged particle multiplicity values of uds jets and gluon jets. The numbers in parentheses are the bin-by-bin correction factors. The uncertainties given for the data include the experimental statistical (first error) and systematic (second error) terms. For the Monte Carlo results, the statistical uncertainties are given. The Jetset 7.4 prediction for 48 GeV jets, obtained by employing an e^+e^- center-of-mass energy of 180 GeV and the same event selection as applied to the other models, is also given.

	$k_\perp$ analysis, $\dfrac{\langle n^{\text{ch.}}\rangle_{\text{gluon}}}{\langle n^{\text{ch.}}\rangle_{\text{b quark}}}$	cone analysis, $\dfrac{\langle n^{\text{ch.}}\rangle_{\text{gluon}}}{\langle n^{\text{ch.}}\rangle_{\text{b quark}}}$	$k_\perp$ analysis, $\dfrac{\langle n^{\text{ch.}}\rangle_{\text{gluon}}}{\langle n^{\text{ch.}}\rangle_{\text{uds quark}}}$	cone analysis, $\dfrac{\langle n^{\text{ch.}}\rangle_{\text{gluon}}}{\langle n^{\text{ch.}}\rangle_{\text{uds quark}}}$
Algebraic correction coeffs.	0.001	0.011	0.018	0.002
Monte Carlo statistics	0.016	0.014	0.026	0.020
Charged particles alone	0.018	0.028	0.000	0.021
Total systematic uncertainty	0.024	0.033	0.032	0.029

Table 6: Breakdown of the contributions to the systematic uncertainty for the ratios of mean charged particle multiplicity between gluon and quark jets.
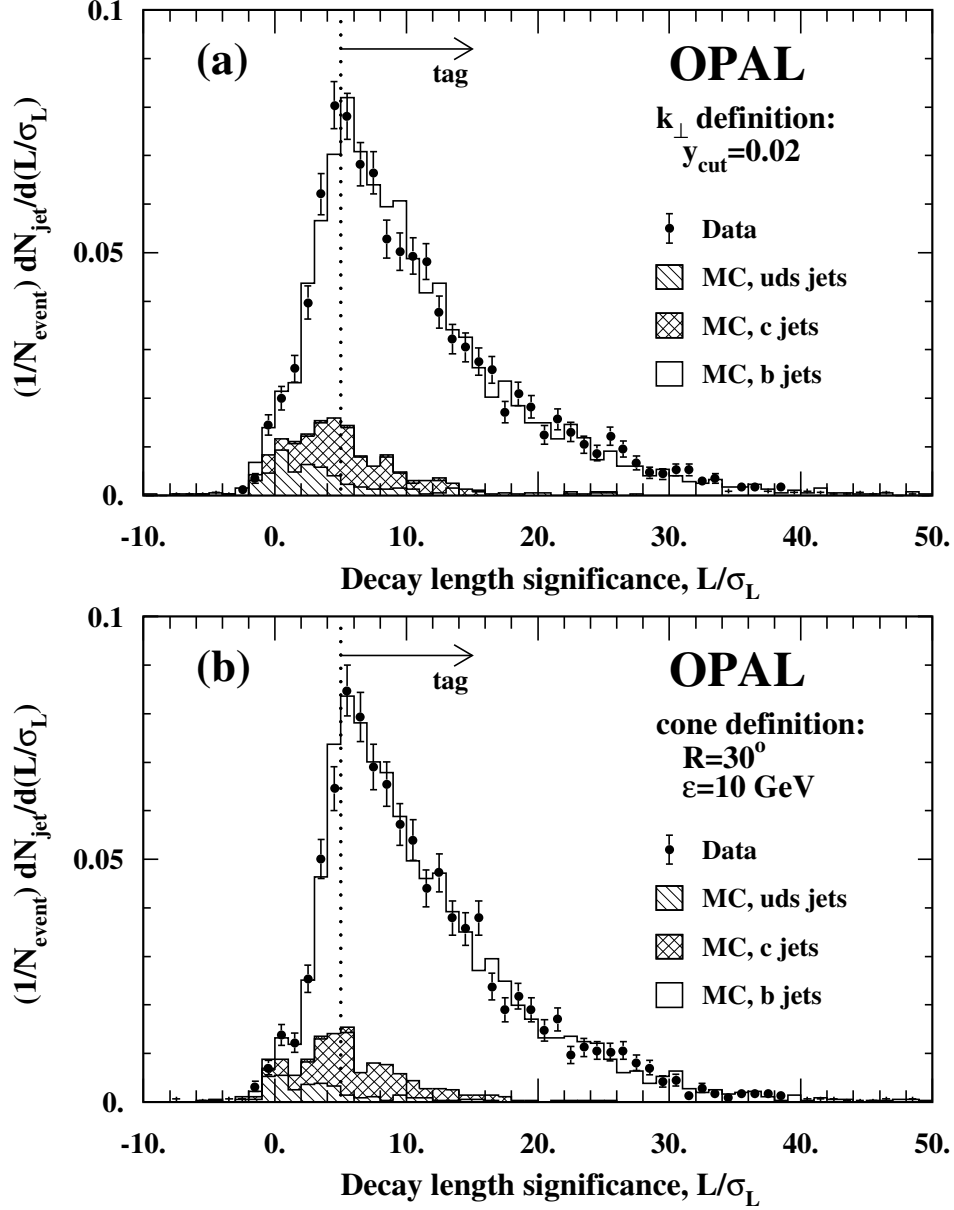
Figure 1: (a) Decay length significance distribution for the highest energy jets of the normal-mixture sample, defined using the $k_\perp$ jet finder, compared to the prediction of the Jetset 7.3 Monte Carlo including detector simulation, after the cuts described in the text have been applied. (b) Corresponding distribution for the cone jet finder.
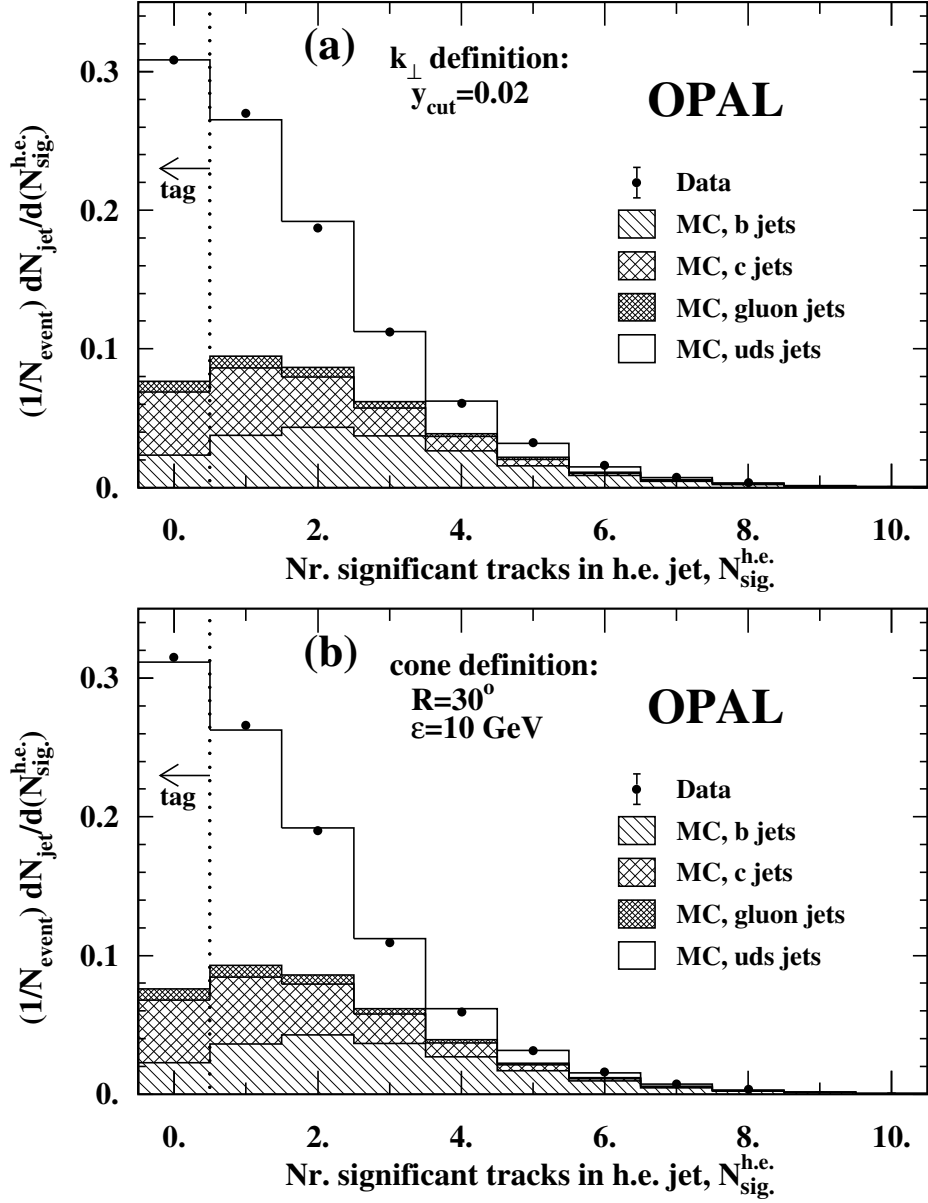
Figure 2: (a) Number of charged tracks with $b/\sigma_b > 2.5$ in the highest energy jets of the normal-mixture sample, after photon conversion candidates have been removed, with jets defined using the $k_\perp$ jet finder. (b) Corresponding distribution for the cone jet finder.
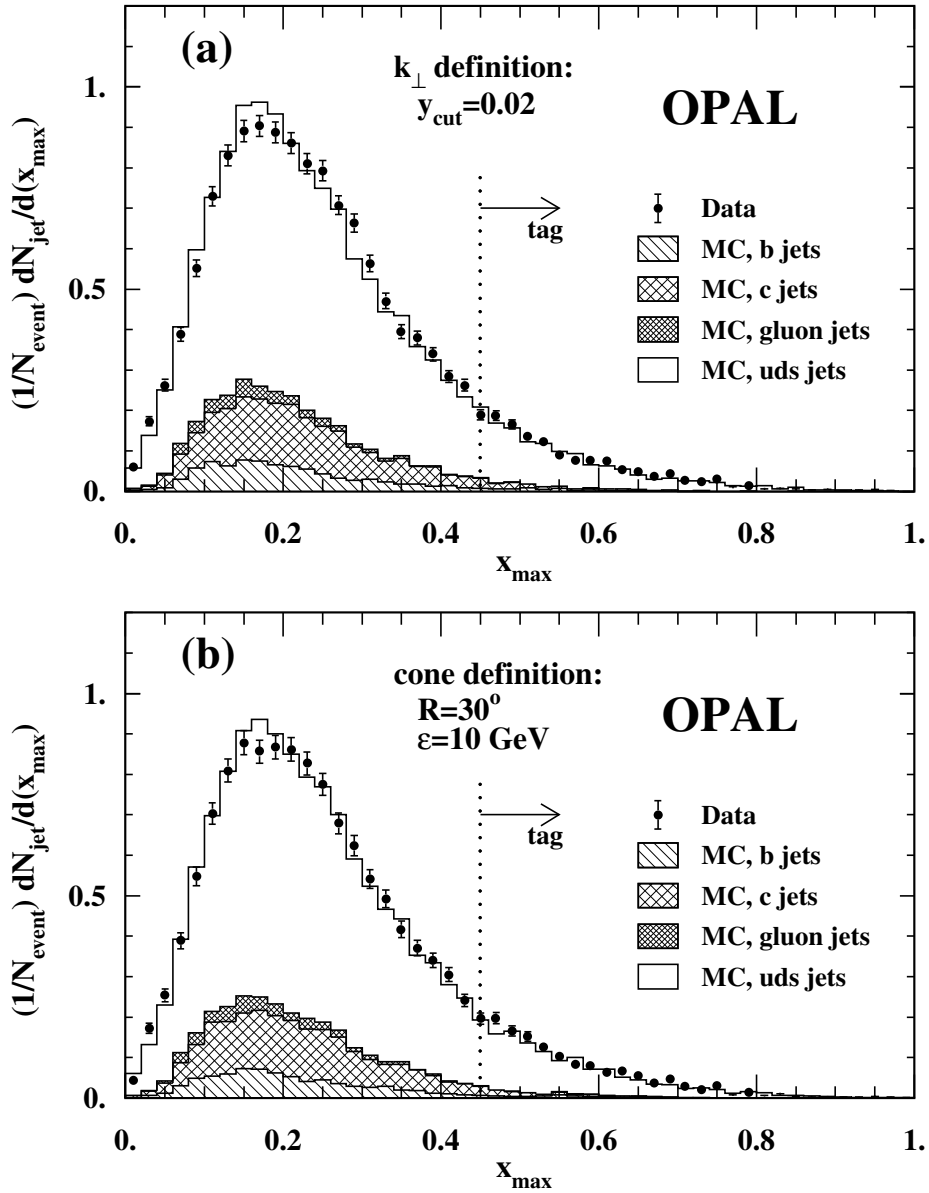
Figure 3: (a) Distribution of the maximum x value of charged tracks in the highest energy jet of the normal-mixture events, where $x = 2 \cdot E/E_{c.m.}$, after events containing tracks with $b/\sigma_b > 2.5$ in the highest energy jets have been removed, with jets defined using the $k_\perp$ jet finder. (b) Corresponding distribution for the cone jet finder.

24
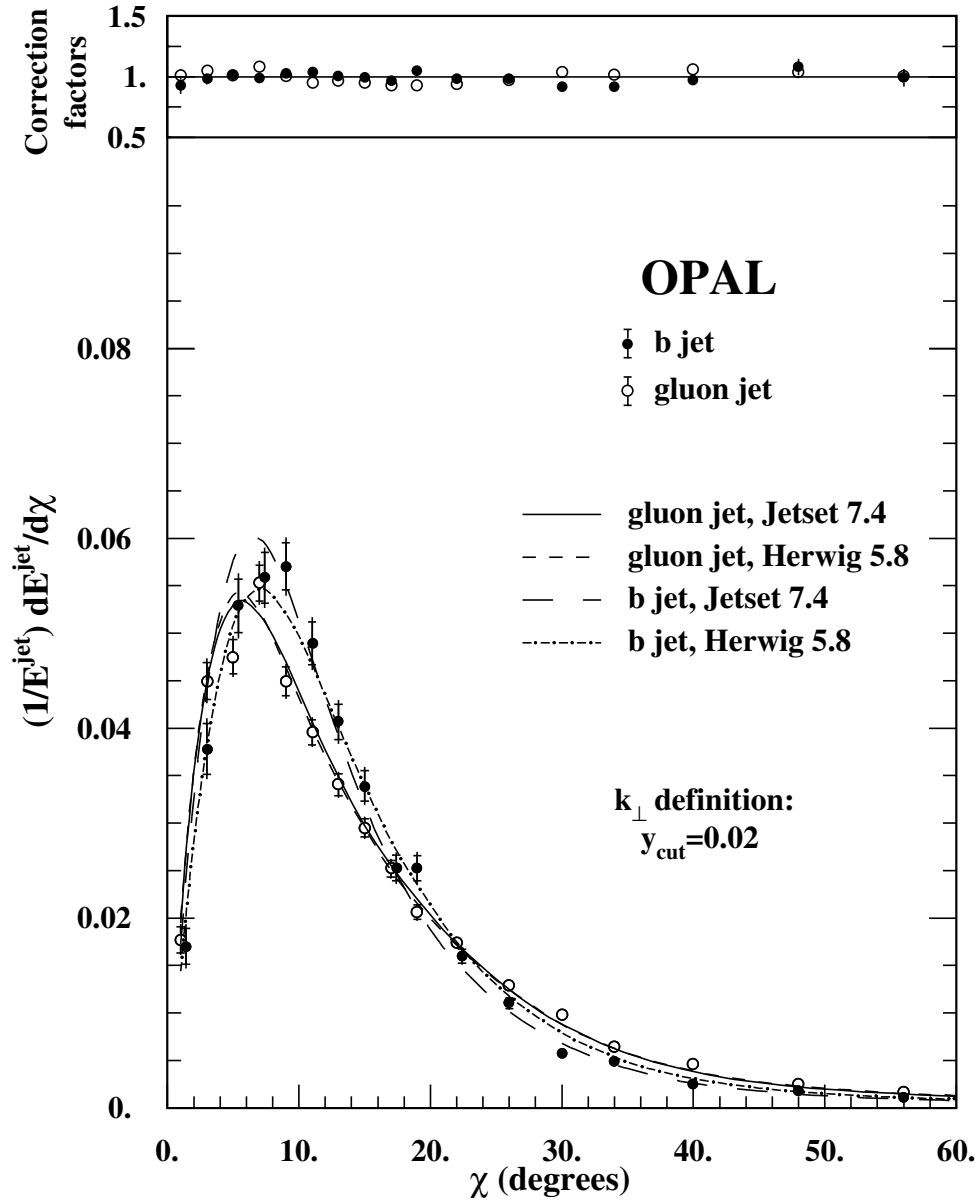
Figure 4: The normalized distribution of jet energy with respect to the jet axis for b and gluon jets defined using the $k_\perp$ jet finder; χ is the angle of a particle with respect to the jet axis. The data have been corrected for gluon and b jet misidentification and for the effects of the detector. The correction factors are shown in the small figure above the data distributions. The errors shown include both the statistical and systematic terms; the experimental statistical uncertaint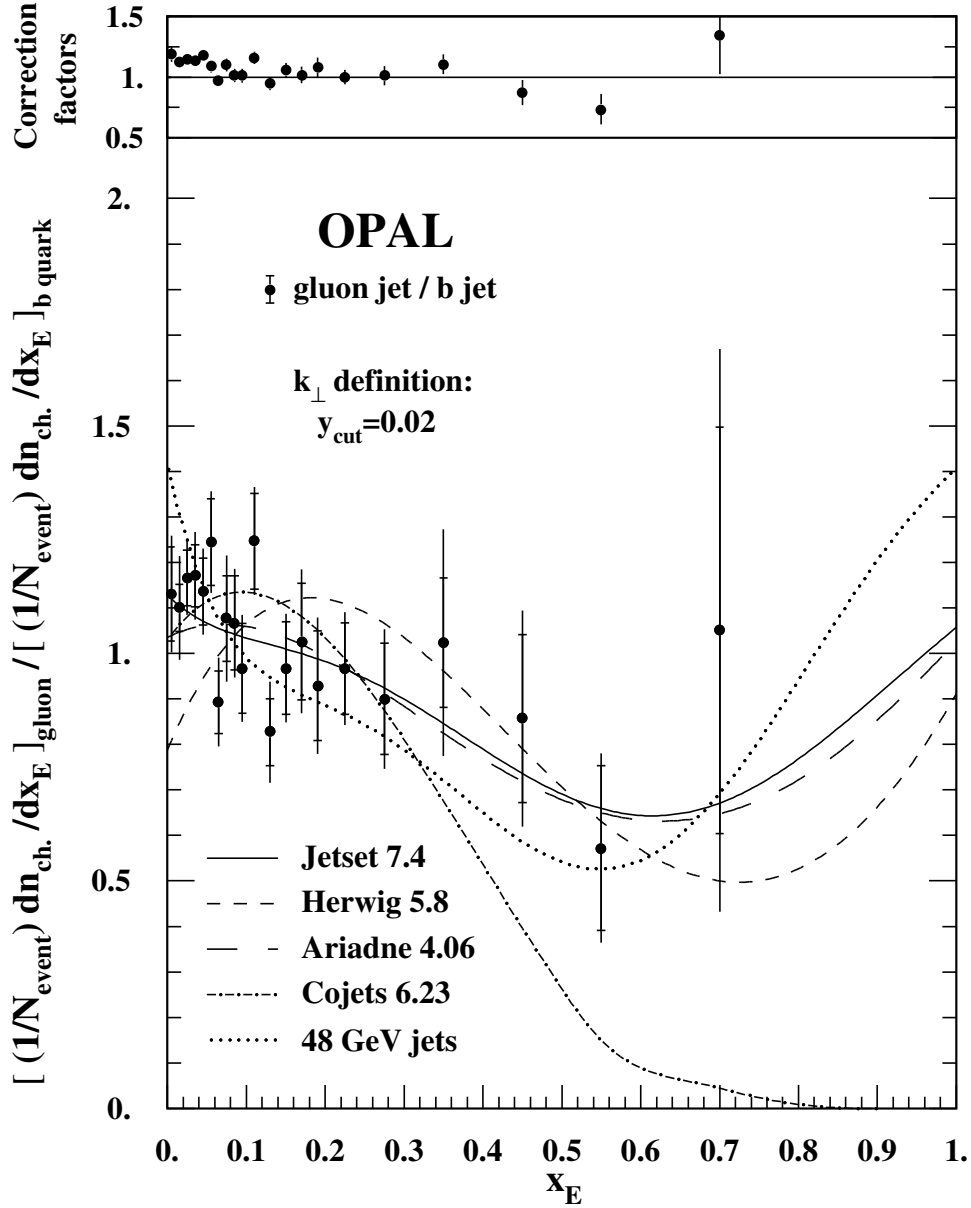ies are indicated by the small horizontal bars. Also shown are the predictions of the Jetset and Herwig QCD shower models.
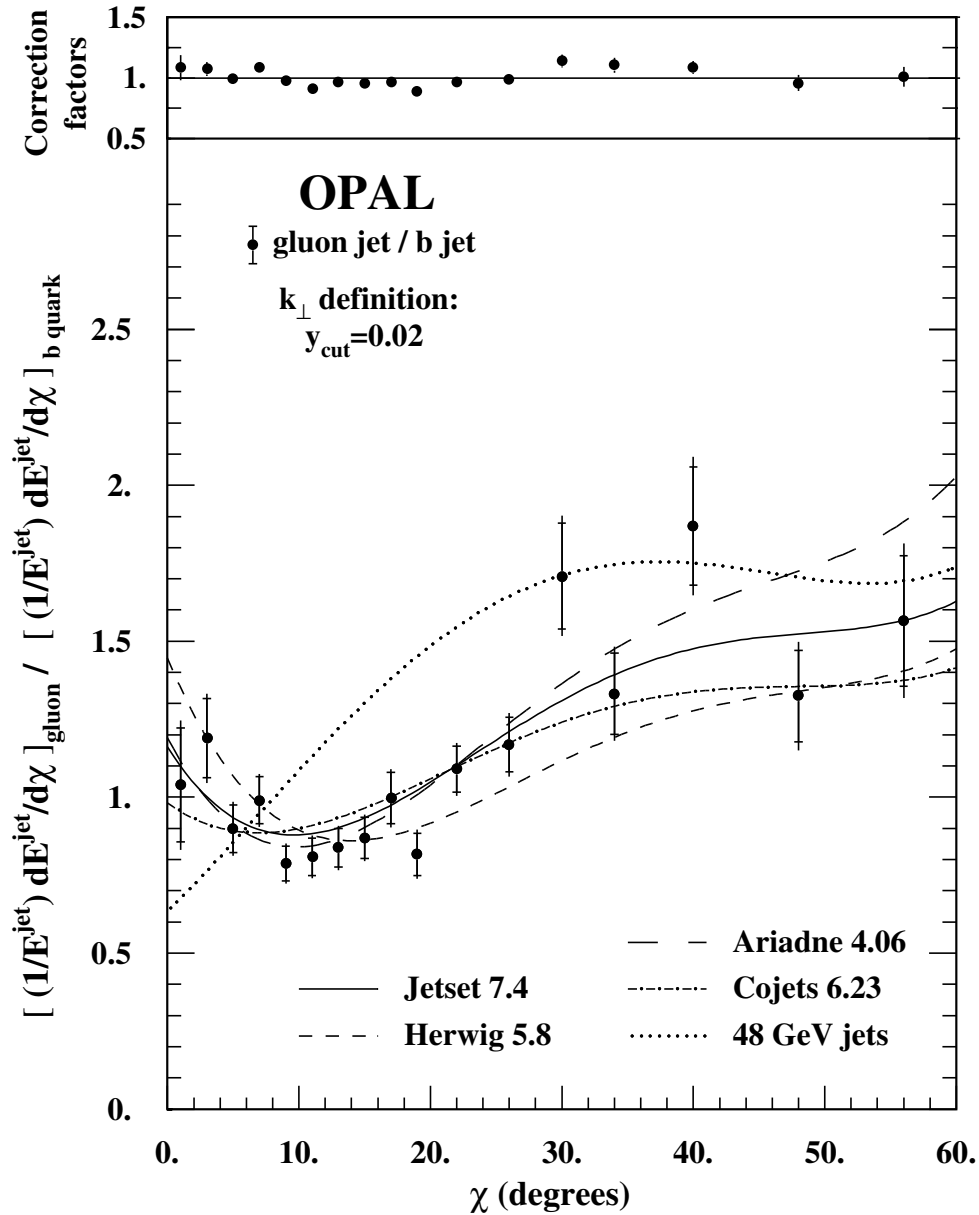
Figure 5: The ratio of the gluon to b jet measurements for the data shown in Fig. 4. The errors shown include both the statistical and systematic terms; the experimental statistical uncertainties are indicated by the small horizontal bars. The predictions of the Ariadne and Cojets QCD shower models are shown along with those of Jetset and Herwig. The Jetset 7.4 prediction for 48 GeV jets, obtained by employing an e^+e^- center-of-mass energy of 180 GeV and the same event selection as applied to the other models, is also shown.
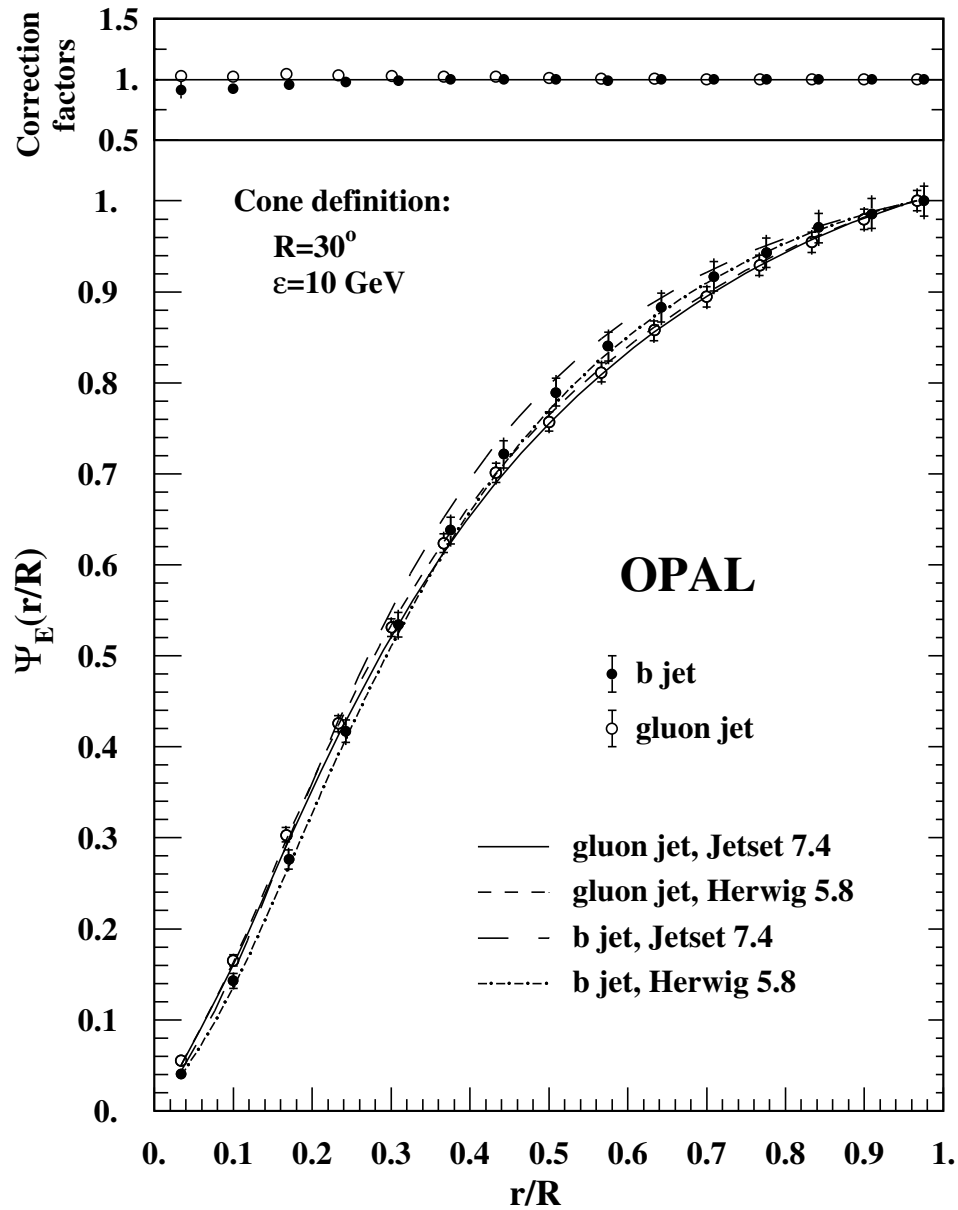
Figure 6: The integral energy profile of gluon and b jets defined using the cone algorithm. The errors shown include both the statistical and systematic terms and are correlated from bin to bin; the experimental statistical uncertainties are indicated by the small horizontal bars.
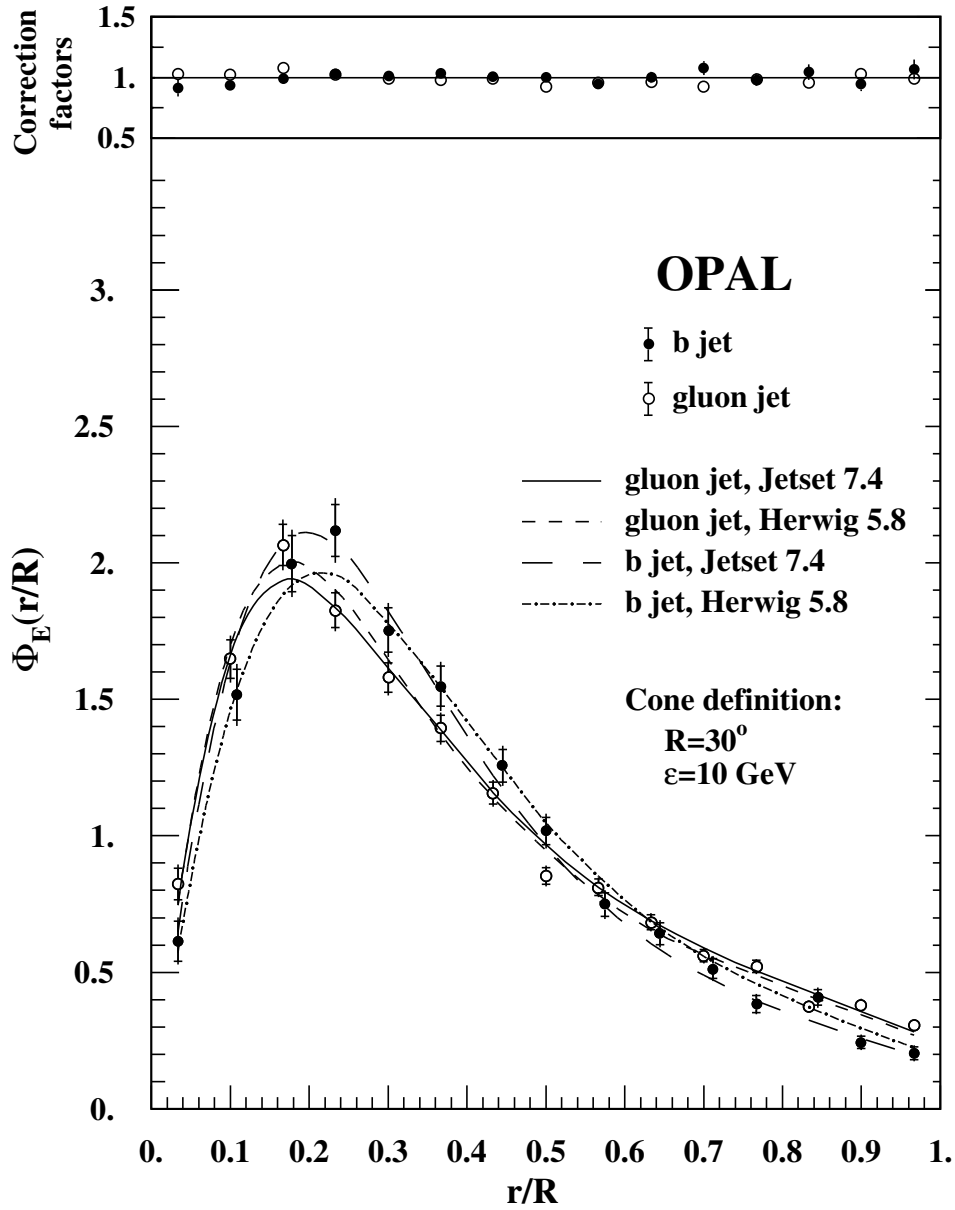
Figure 7: The differential energy profile of gluon and b jets defined using the cone algorithm. The errors shown include both the statistical and systematic terms; the experimental statistical uncertainties are indicated by the small horizontal bars.
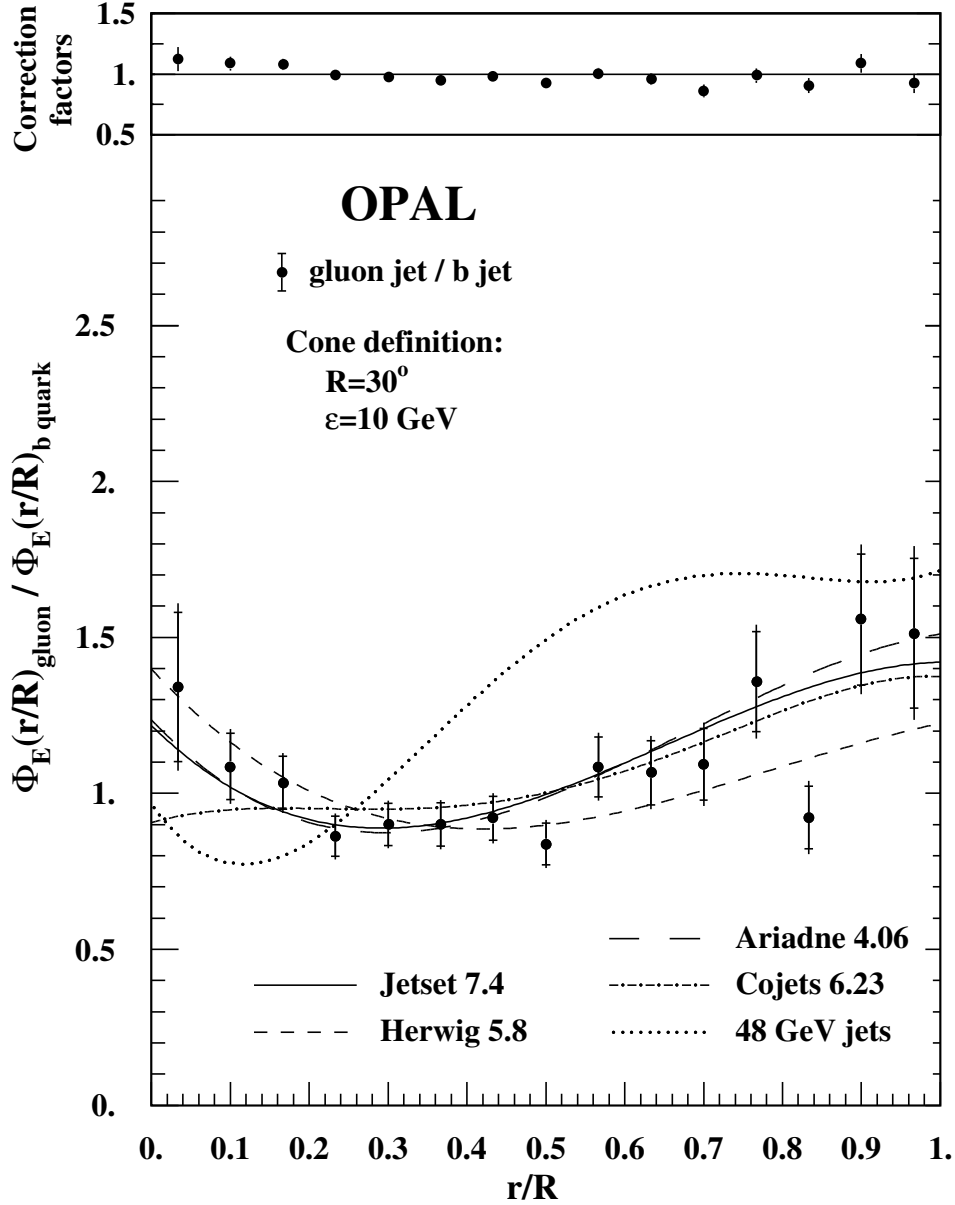
Figure 8: The ratio of the distributions shown in Fig. 7. The errors shown include both the statistical and systematic terms; the experimental statistical uncertainties are indicated by the small horizontal bars. The Jetset 7.4 prediction for 48 GeV jets, obtained by employing an e^+e^- center-of-mass energy of 180 GeV and the same event selection as applied to the other models, is also shown.
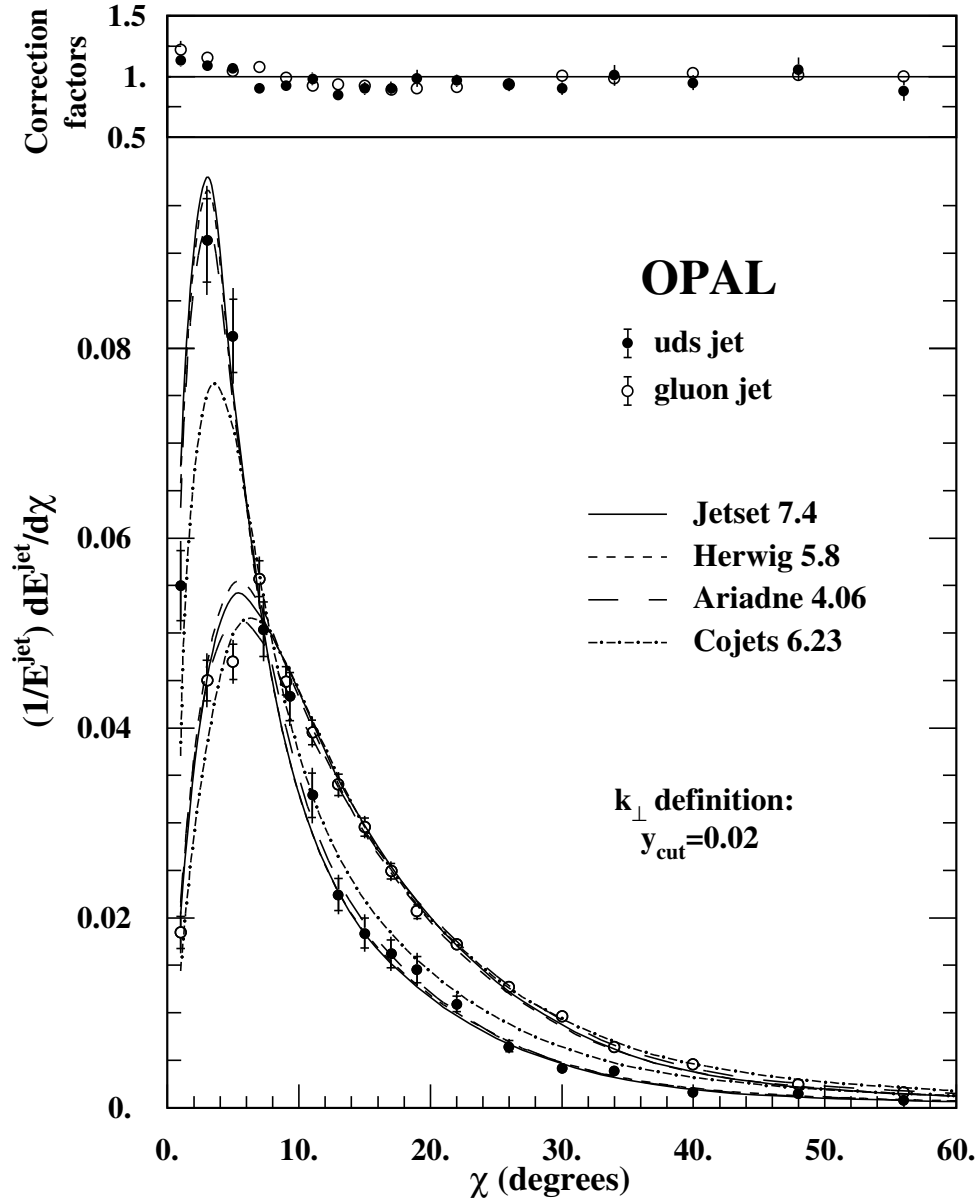
29
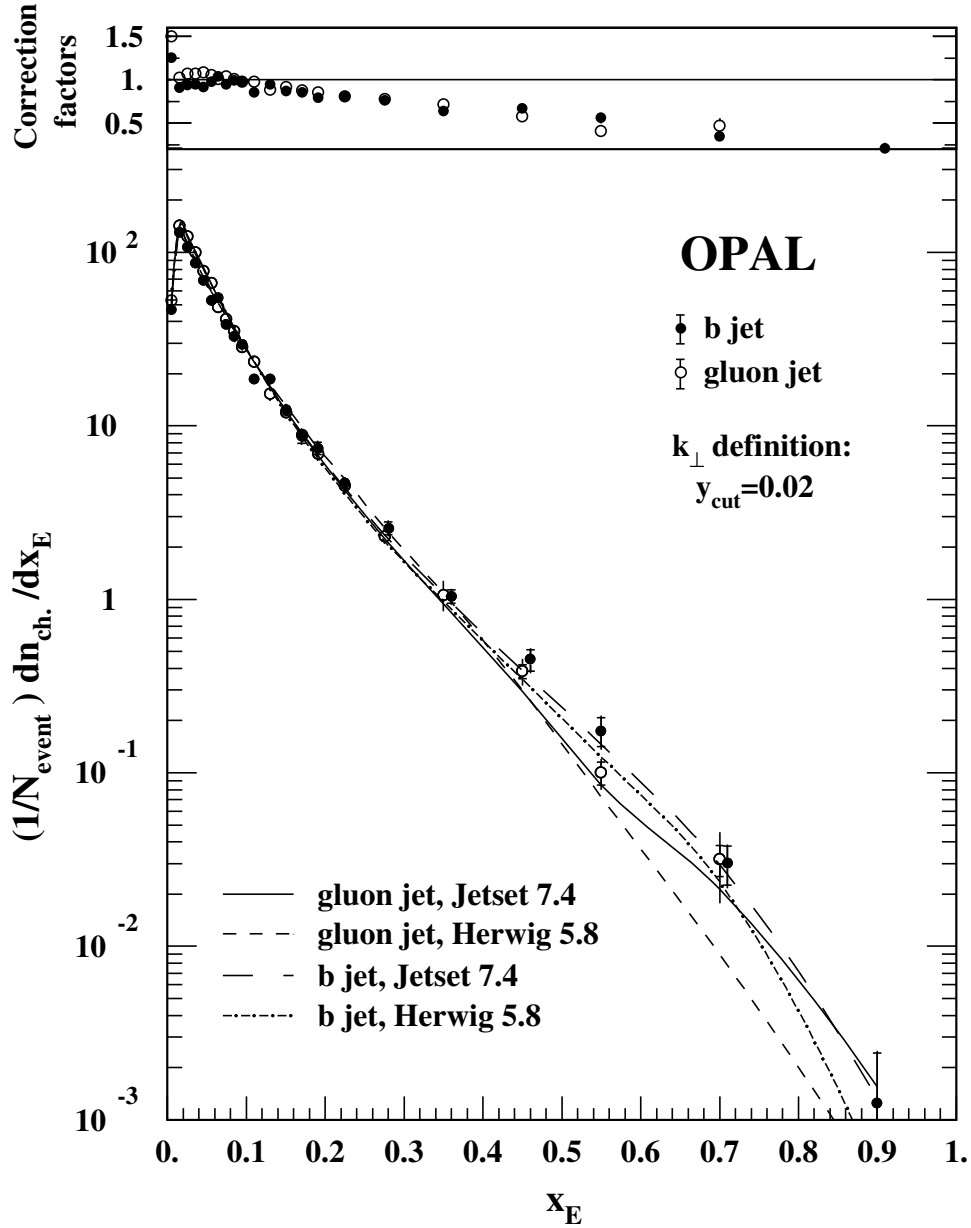
Figure 9: Charged particle fragmentation functions of gluon and b jets defined using the $k_\perp$ jet finder. The errors shown include both the statistical and systematic terms; the experimental statistical uncertainties are indicated by the small horizontal bars.
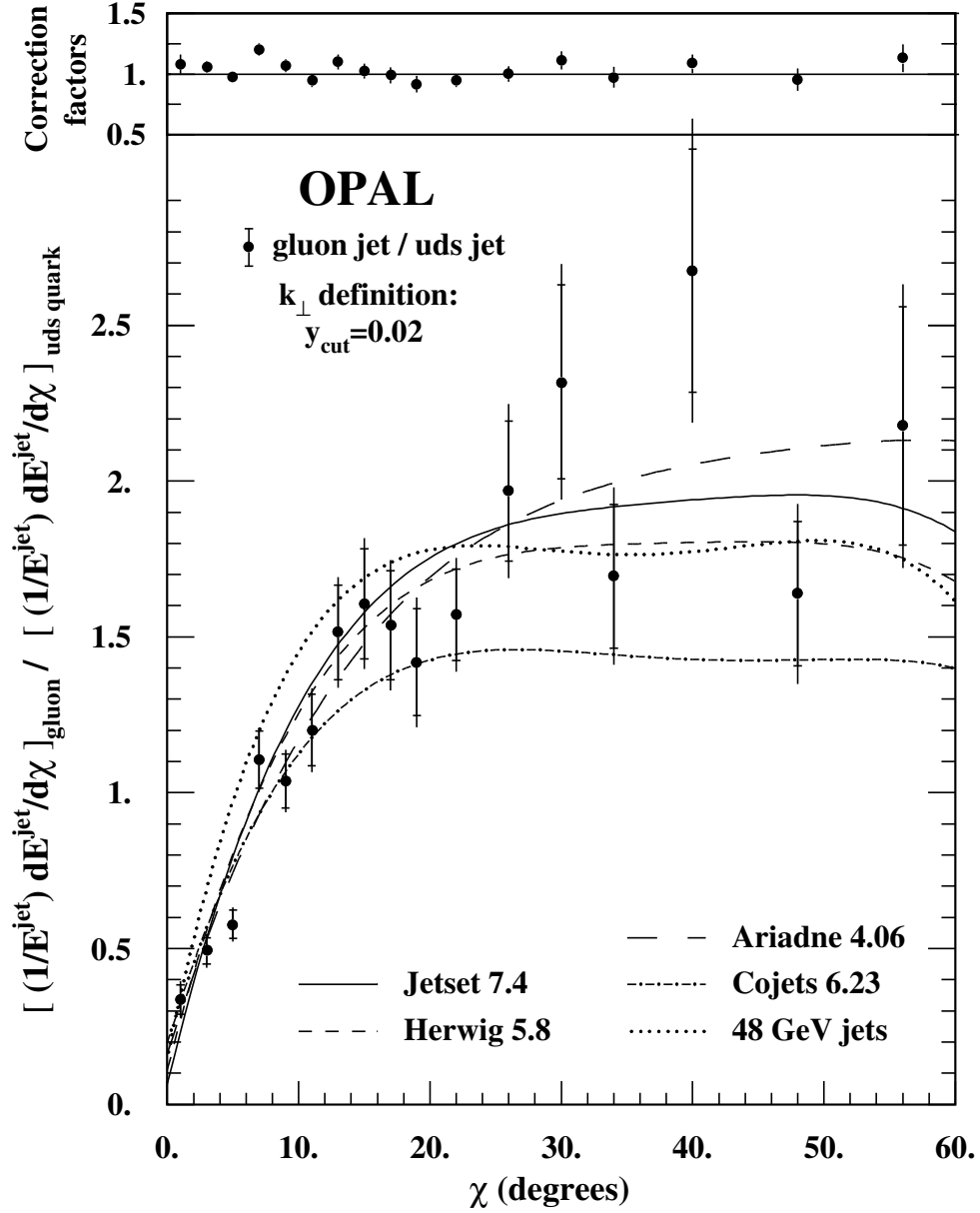
30

Figure 10: The ratio of the distributions shown in Fig. 9. The errors shown include both the statistical and systematic terms; the experimental statistical uncertainties are indicated by the small horizontal bars. The Jetset 7.4 prediction for 48 GeV jets, obtained by employing an e^+e^- center-of-mass energy of 180 GeV and the same event selection as applied to the other models, is also shown.
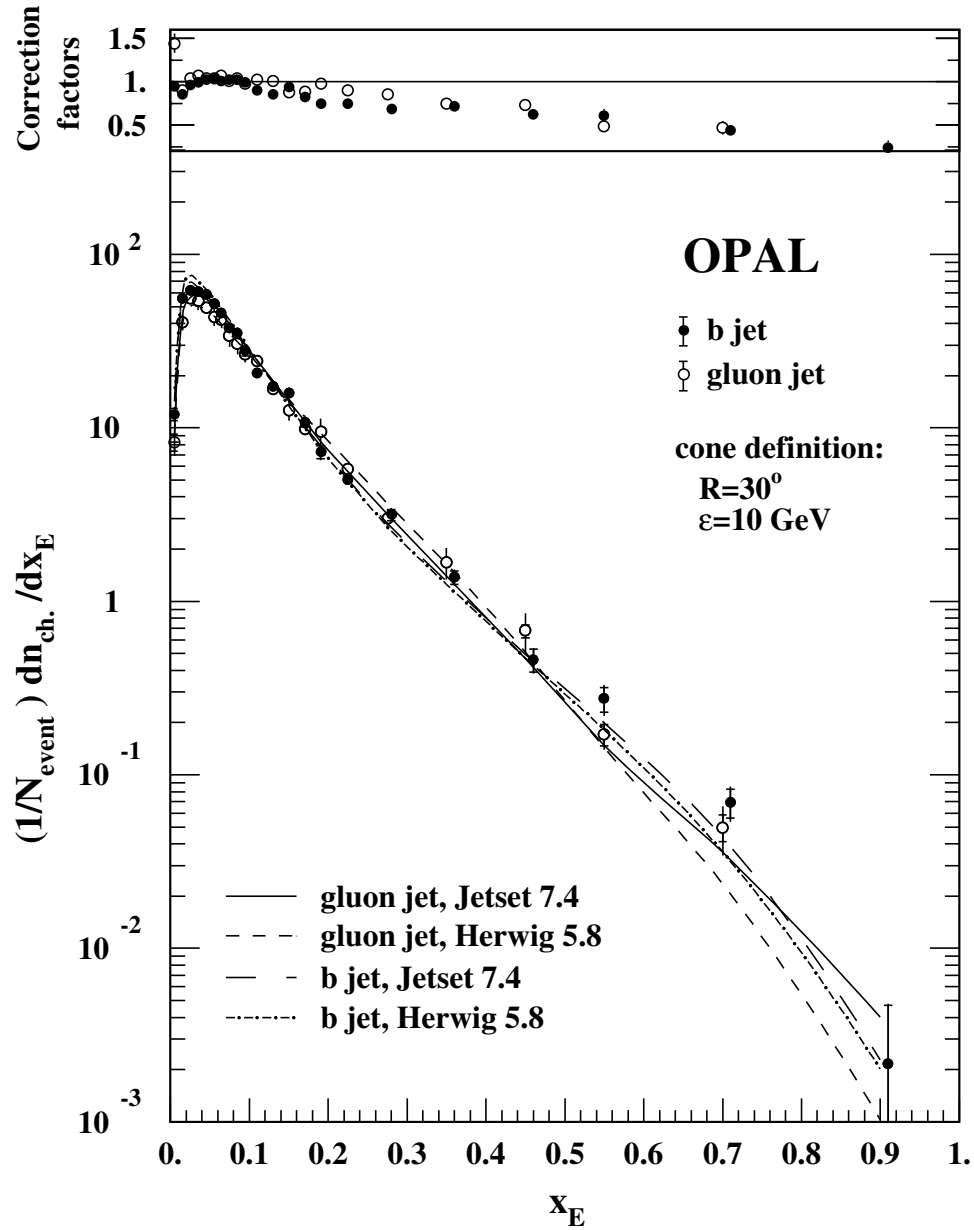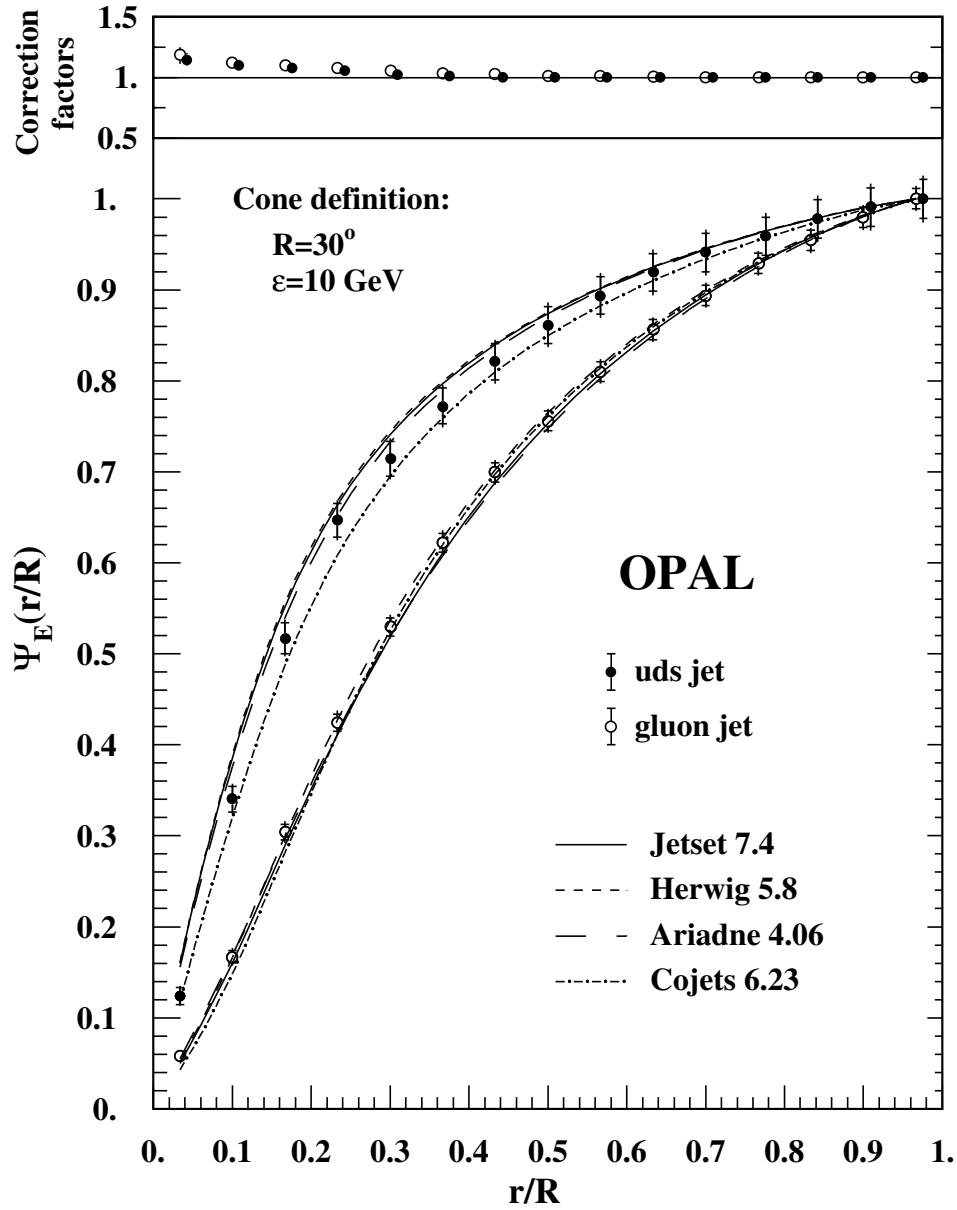
Figure 11: Charged particle fragmentation functions of gluon and b jets defined using the cone jet finder. The errors shown include both the statistical and systematic terms; the experimental statistical uncertainties are indicated by the small horizontal bars.
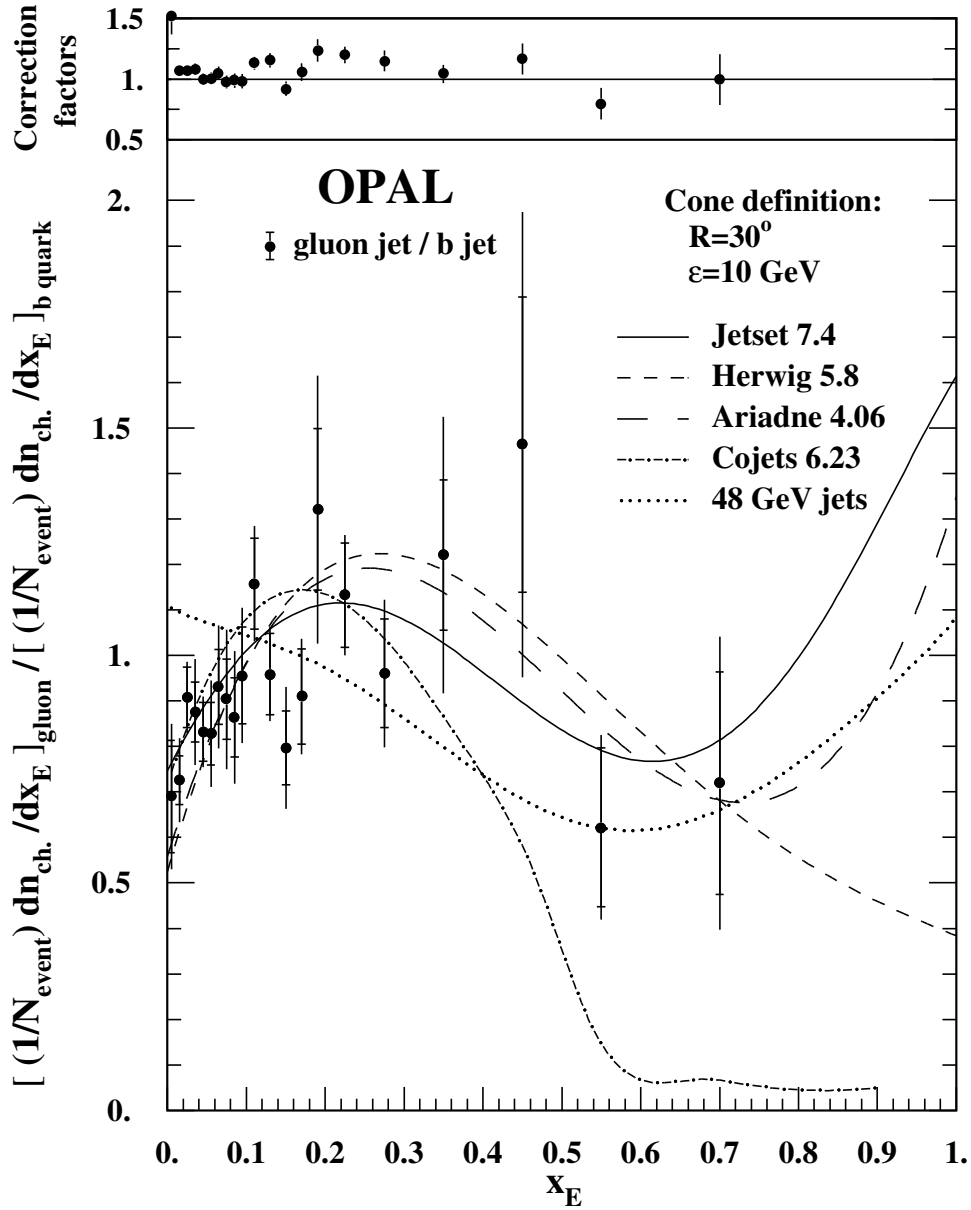
Figure 12: The ratio of the distributions shown in Fig. 11. The errors shown include both the statistical and systematic terms; the experimental statistic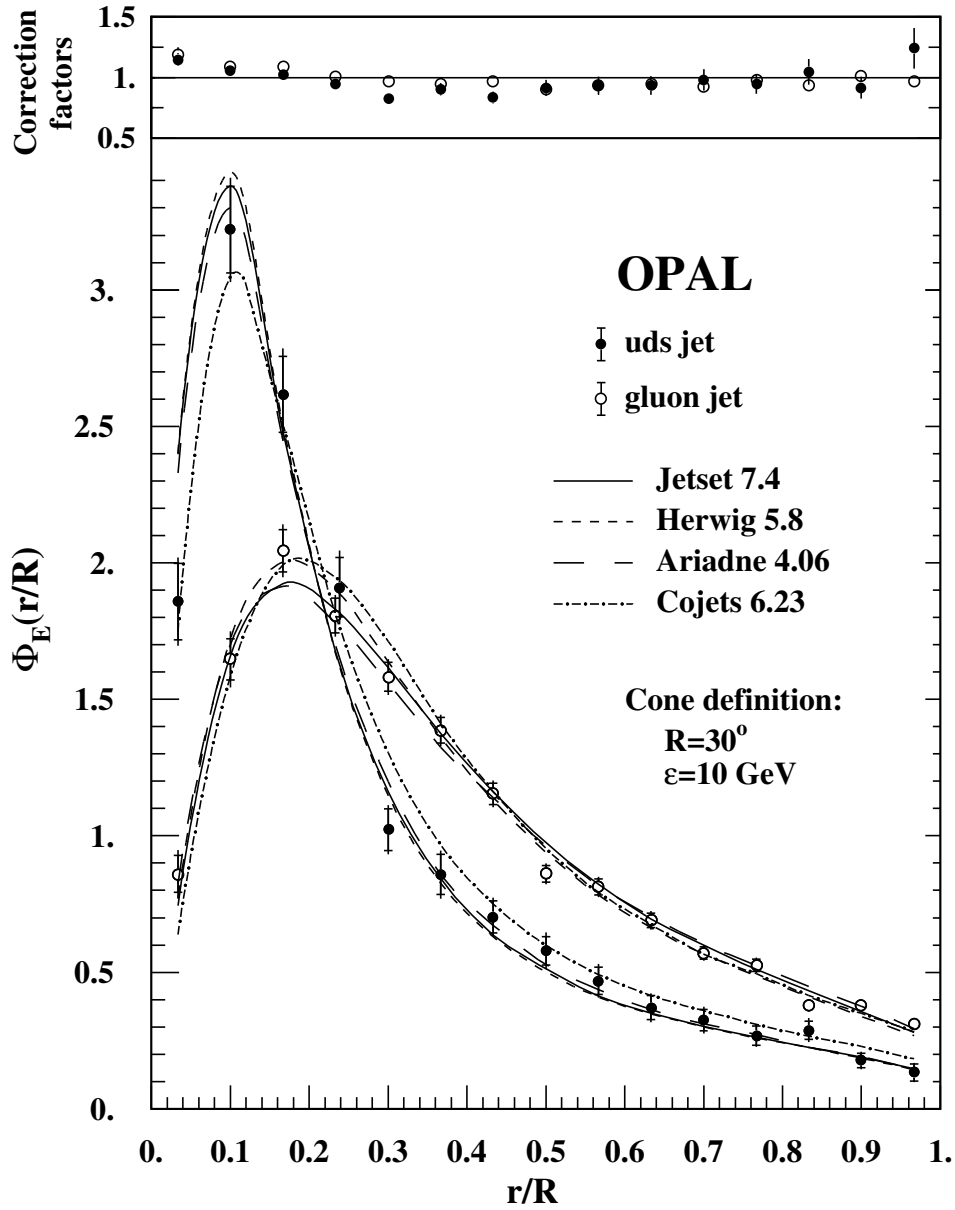al uncertainties are indicated by the small horizontal bars. The Jetset 7.4 prediction for 48 GeV jets, obtained by employing an e^+e^- center-of-mass energy of 180 GeV and the same event selection as applied to the other models, is also shown.

Figure 13: The normalized distribution of jet energy with respect to the jet axis for uds and gluon jets defined using the $k_\perp$ jet finder; The errors shown include both the statistical and systematic terms; the experimental statistical uncertainties are indicated by the small horizontal bars.
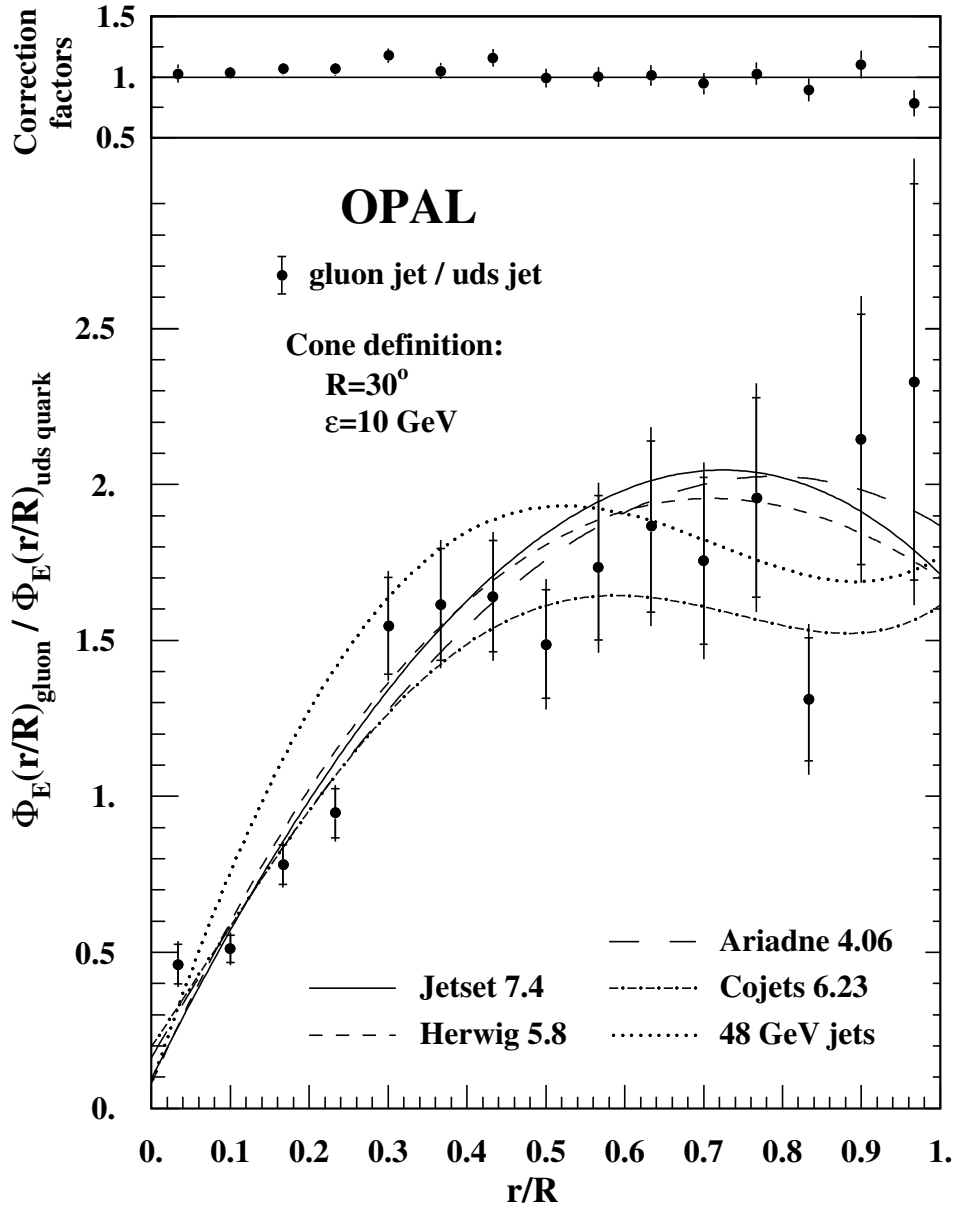
Figure 14: The ratio of the gluon to uds jet measurements for the data shown in Fig. 13. The errors shown include both the statistical and systematic terms; the experimental statistical uncertainties are indicated by the small horizontal bars. The Jetset 7.4 prediction for 48 GeV jets, obtained by employing an e^+e^- center-of-mass energy of 180 GeV and the same event selection as applied to the other models, is also shown.

Figure 15: The integral energy profile of gluon and uds jets defined using the cone algorithm. The errors shown include both the statistical and systematic terms and are correlated from bin to bin; the experimental statistical uncertainties are indicated by the small horizontal bars.

Figure 16: The differential energy profile of gluon and uds jets defined using the cone algorithm. The errors shown include both the statistical and systematic terms; the experimental statistical uncertainties are indicated by the small horizontal bars.
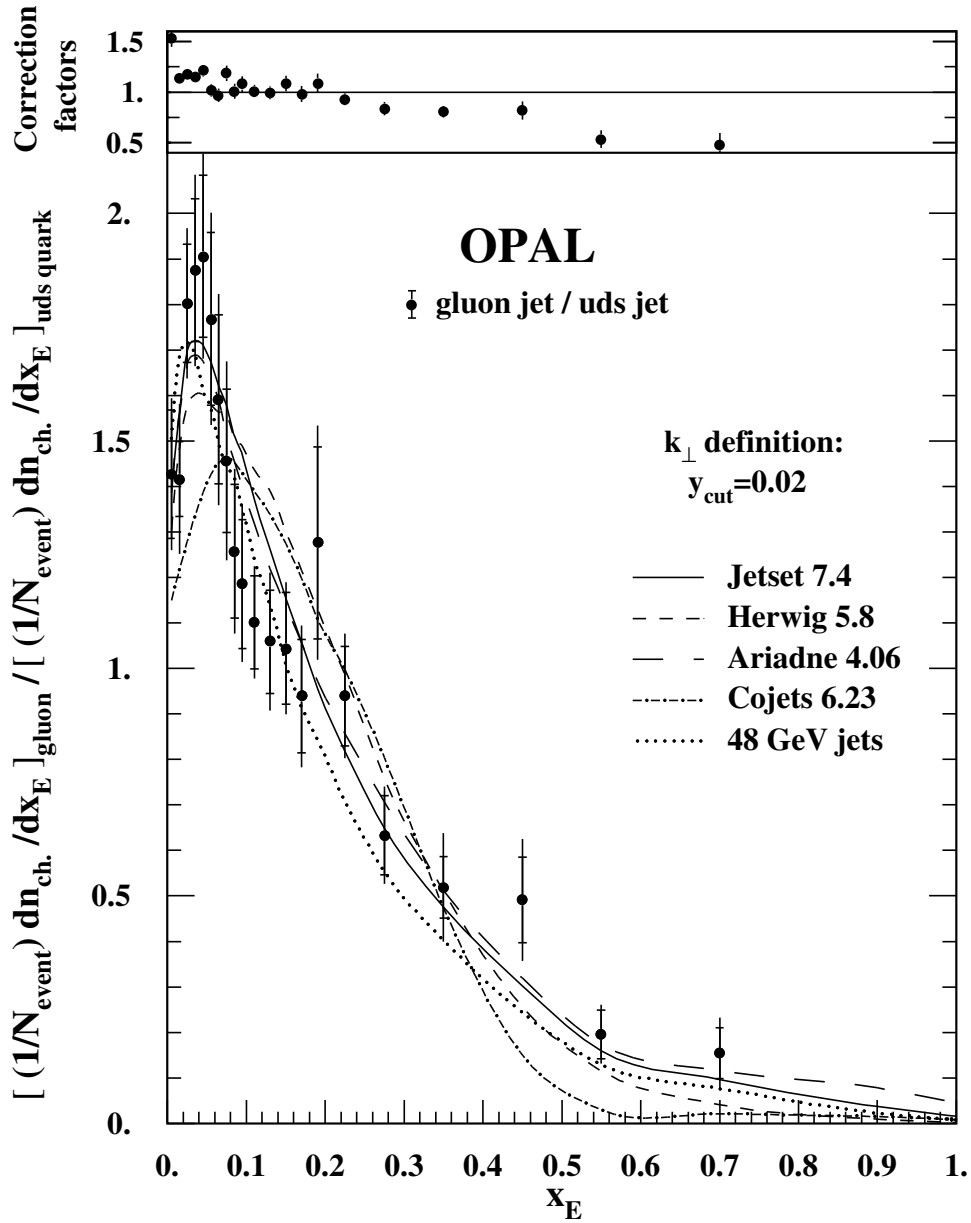
Figure 17: The ratio of the distributions shown in Fig. 16. The errors shown include both the statistical and systematic terms; the experimental statistical uncertainties are indicated by the small horizontal bars. The Jetset 7.4 prediction for 48 GeV jets, obtained by employing an e^+e^- center-of-mass energy of 180 GeV and the same event selection as applied to the other models, is also shown.
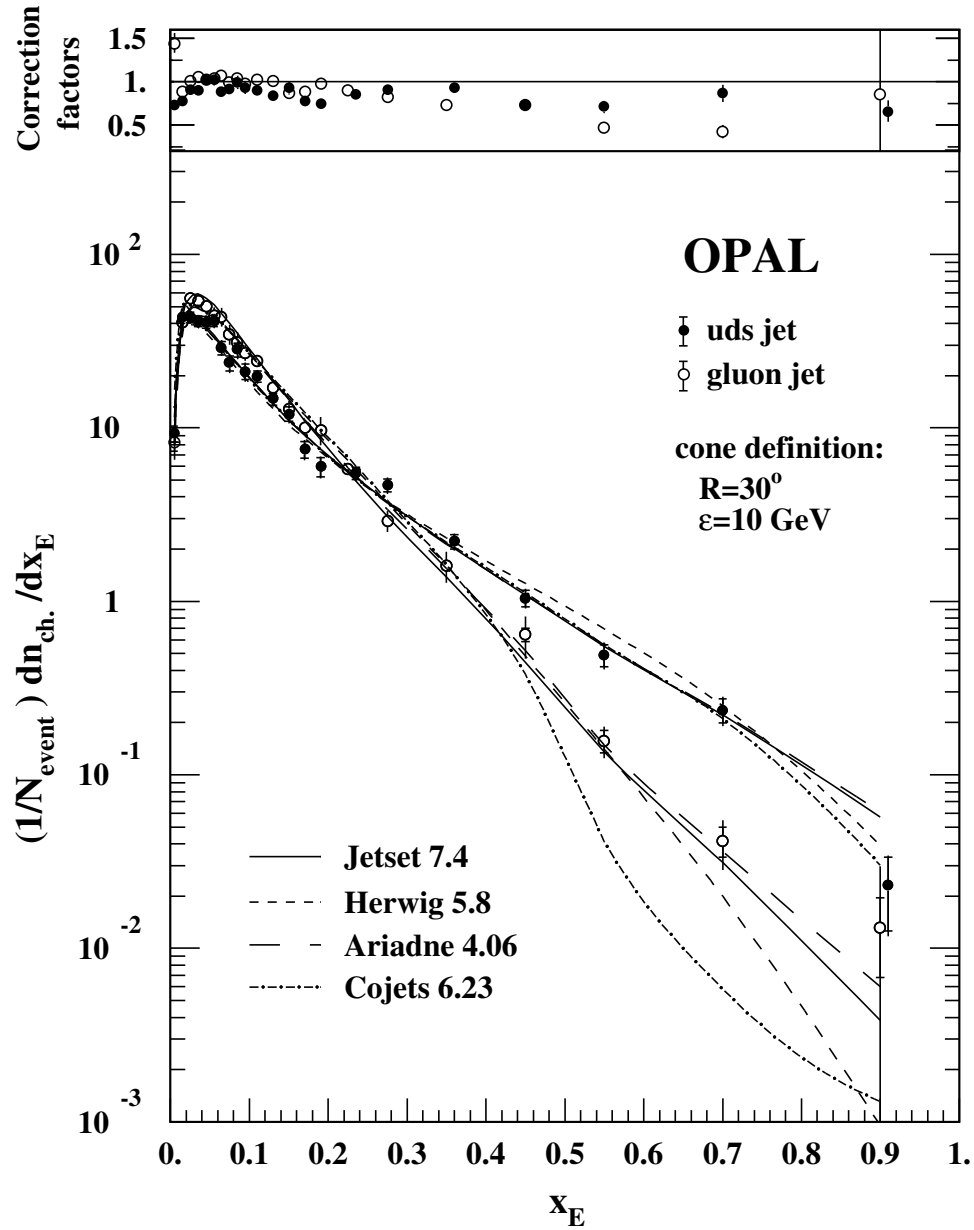
38
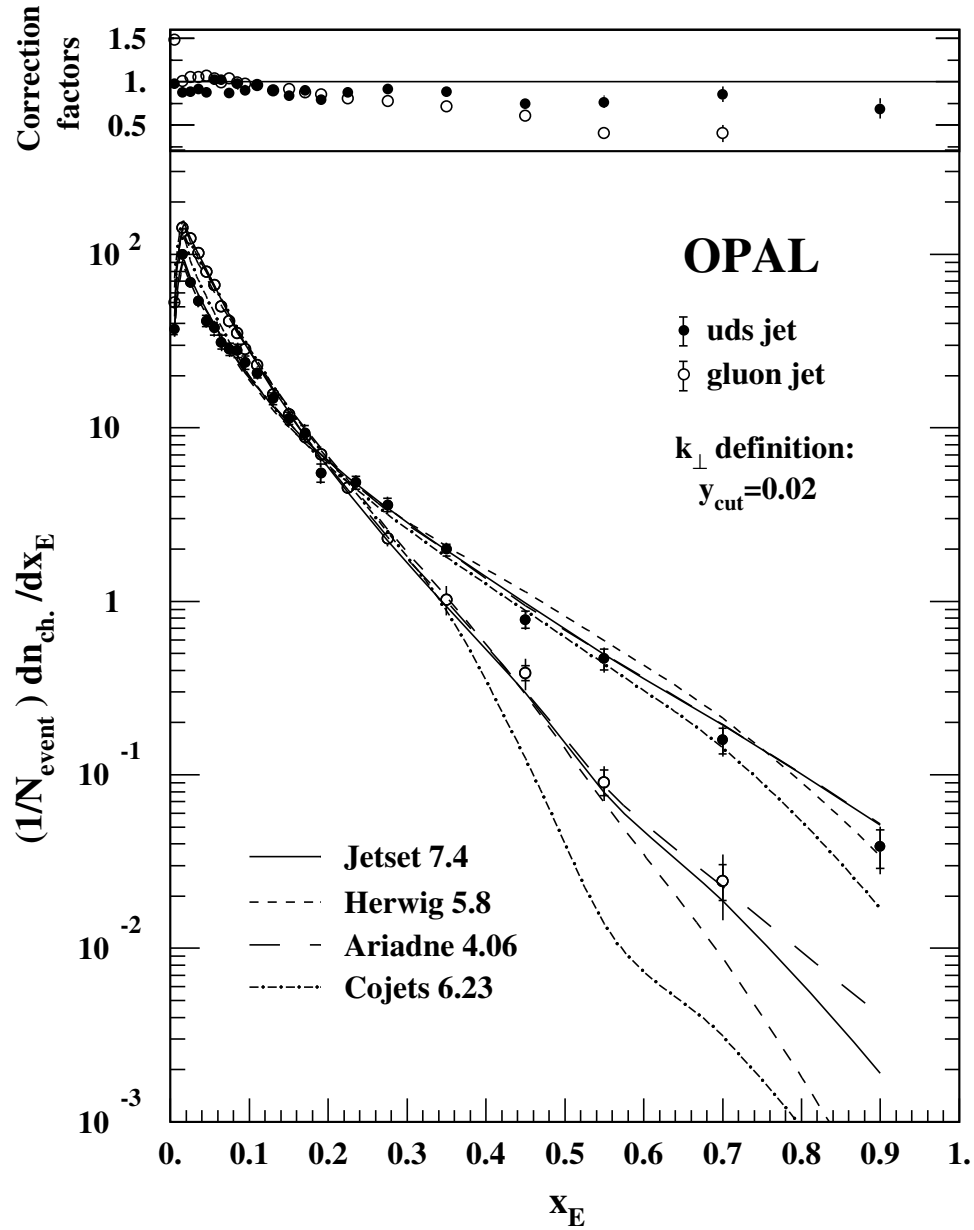
Figure 18: Charged particle fragmentation functions of gluon and uds jets defined using the $k_\perp$ jet finder. The errors shown include both the statistical and systematic terms; the experimental statistical uncertainties are indicated by the small horizontal bars.
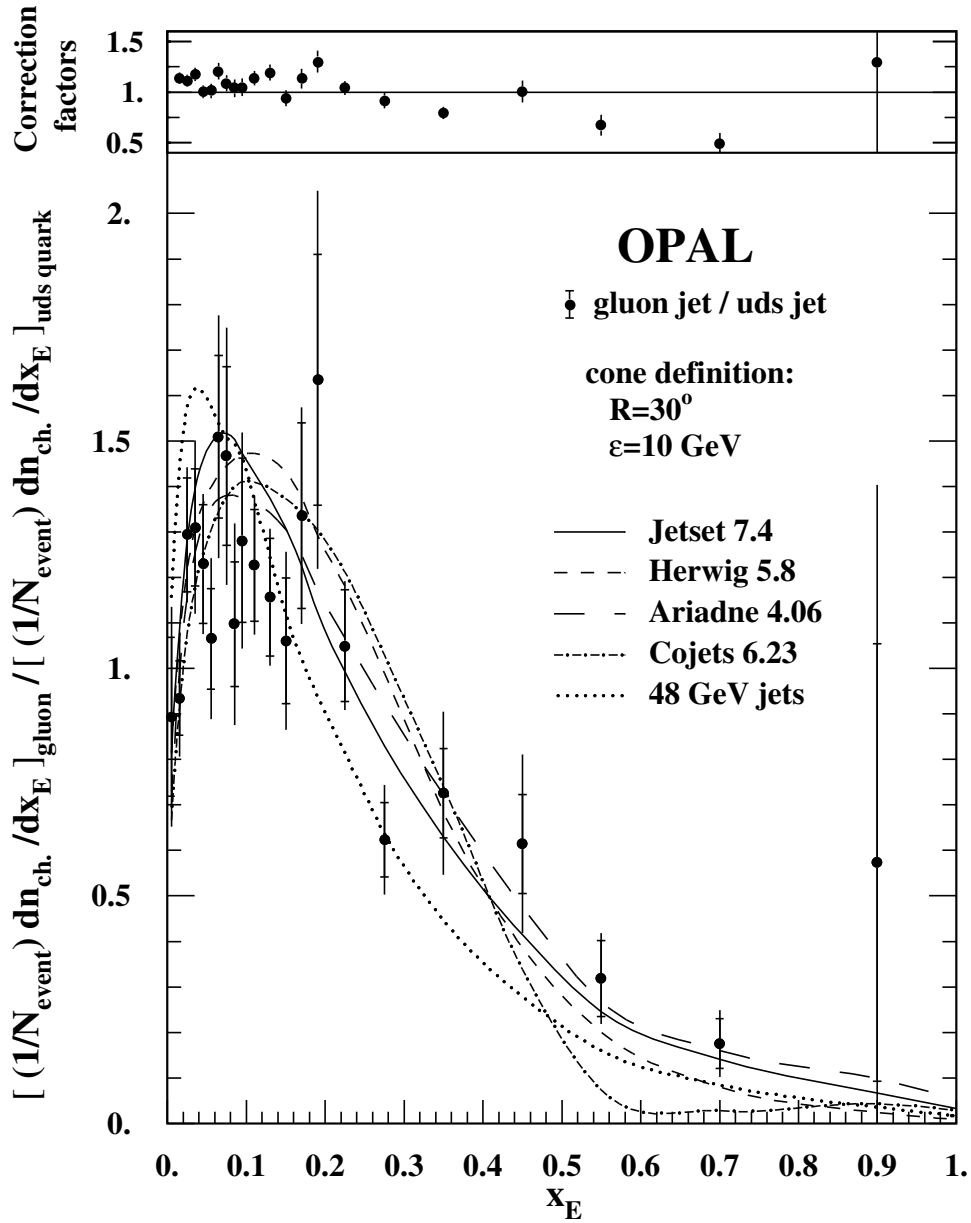
Figure 19: The ratio of the distributions shown in Fig. 18. The errors shown include both the statistical and systematic terms; the experimental statistical uncertainties are indicated by the small horizontal bars. The Jetset 7.4 prediction for 48 GeV jets, obtained by employing an e^+e^- center-of-mass energy of 180 GeV and the same event selection as applied to the other models, is also shown.

40

Figure 20: Charged particle fragmentation functions of gluon and uds jets defined using the cone jet finder. The errors shown include both the statistical and systematic terms; the experimental statistical uncertainties are indicated by the small horizontal bars.

Figure 21: The ratio of the distributions shown in Fig. 20. The errors shown include both the statistical and systematic terms; the experimental statistical uncertainties are indicated by the small horizontal bars. The Jetset 7.4 prediction for 48 GeV jets, obtained by employing an e^+e^- center-of-mass energy of 180 GeV and the same event selection as applied to the other models, is also shown.
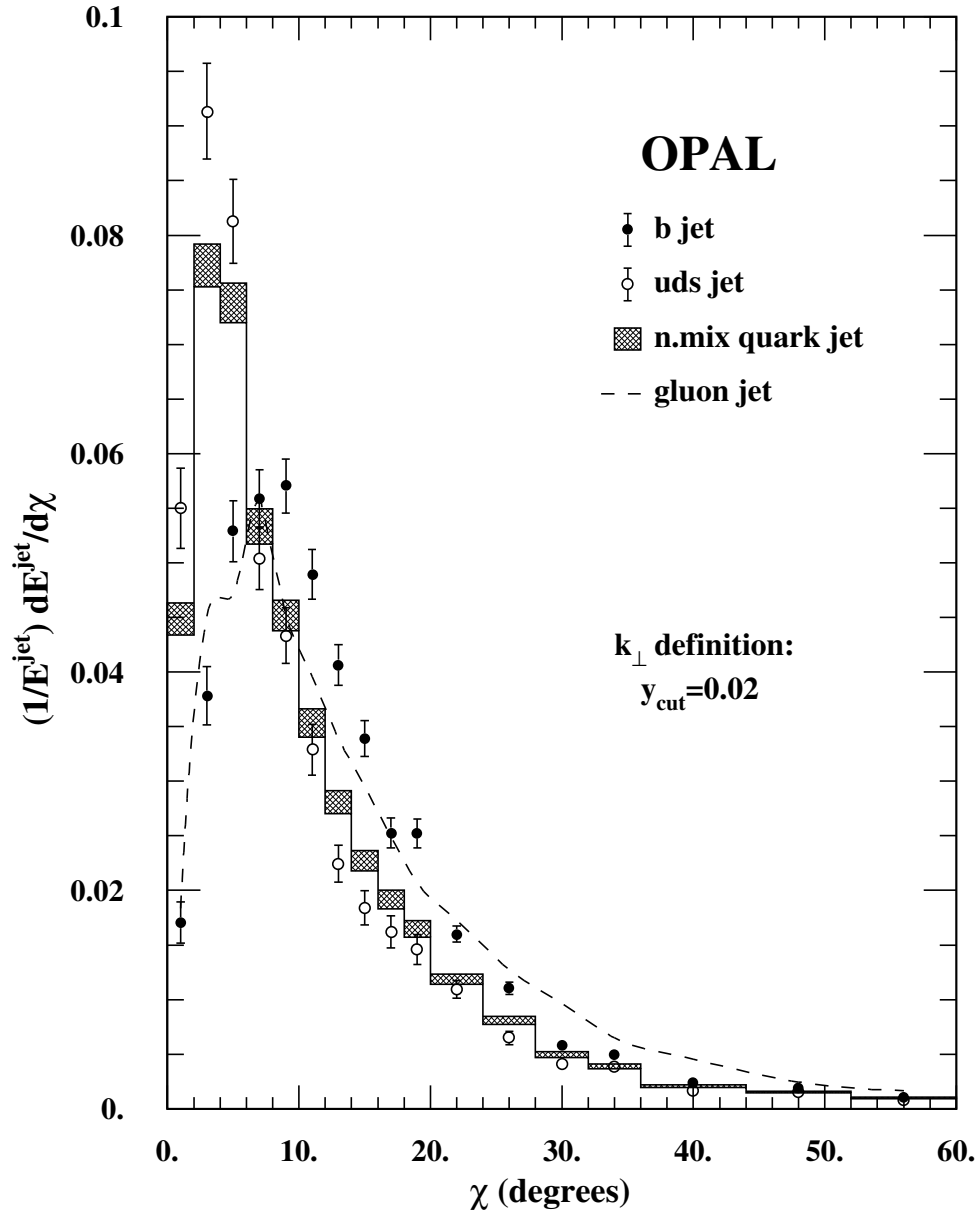
Figure 22: Comparison of b jet, uds jet, normal-mixture quark jet and gluon jet data for the normalized distribution of jet energy with respect to the jet axis, defined using the $k_\perp$ jet finder. The errors show the experimental statistical uncertainties.
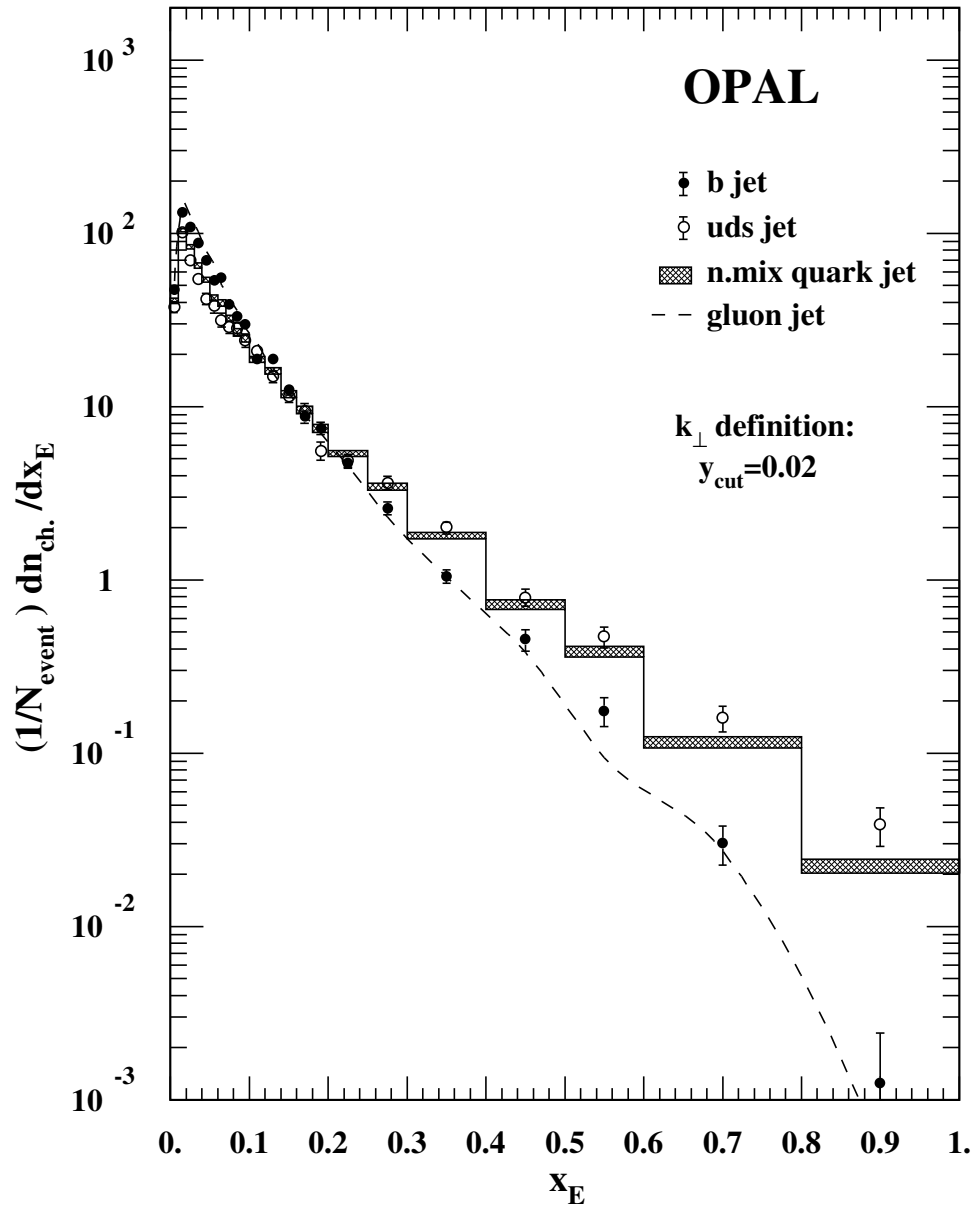
43

Figure 23: Comparison of b jet, uds jet, normal-mixture quark jet and gluon jet data for the charged particle fragmentation function, defined using the $k_\perp$ jet finder. The errors show the experimental statistical uncertainties.
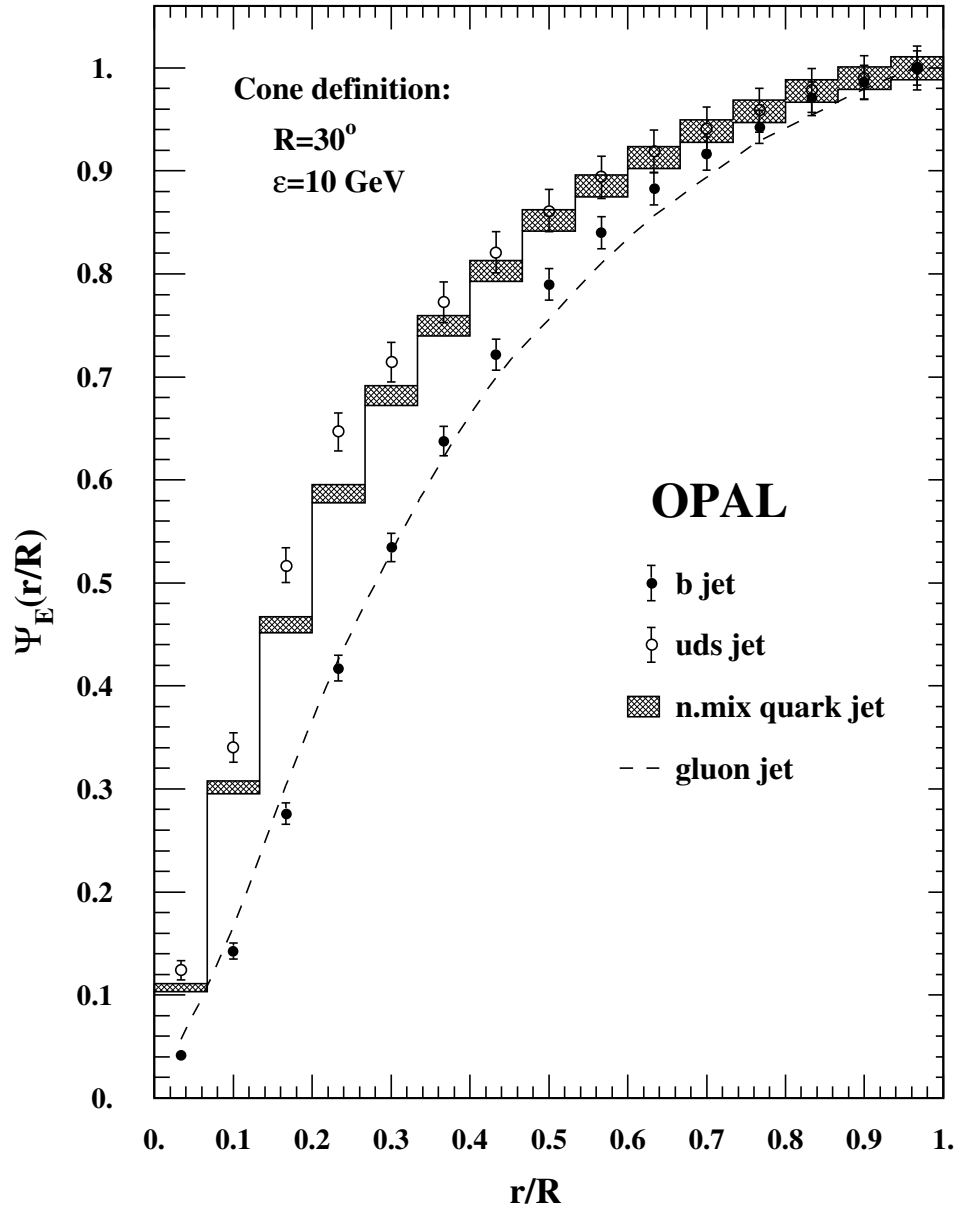
Figure 24: Comparison of b jet, uds jet, normal-mixture quark jet and gluon jet data for the integral energy profile, defined using the cone jet finder. The errors show the experimental statistical uncertainties.
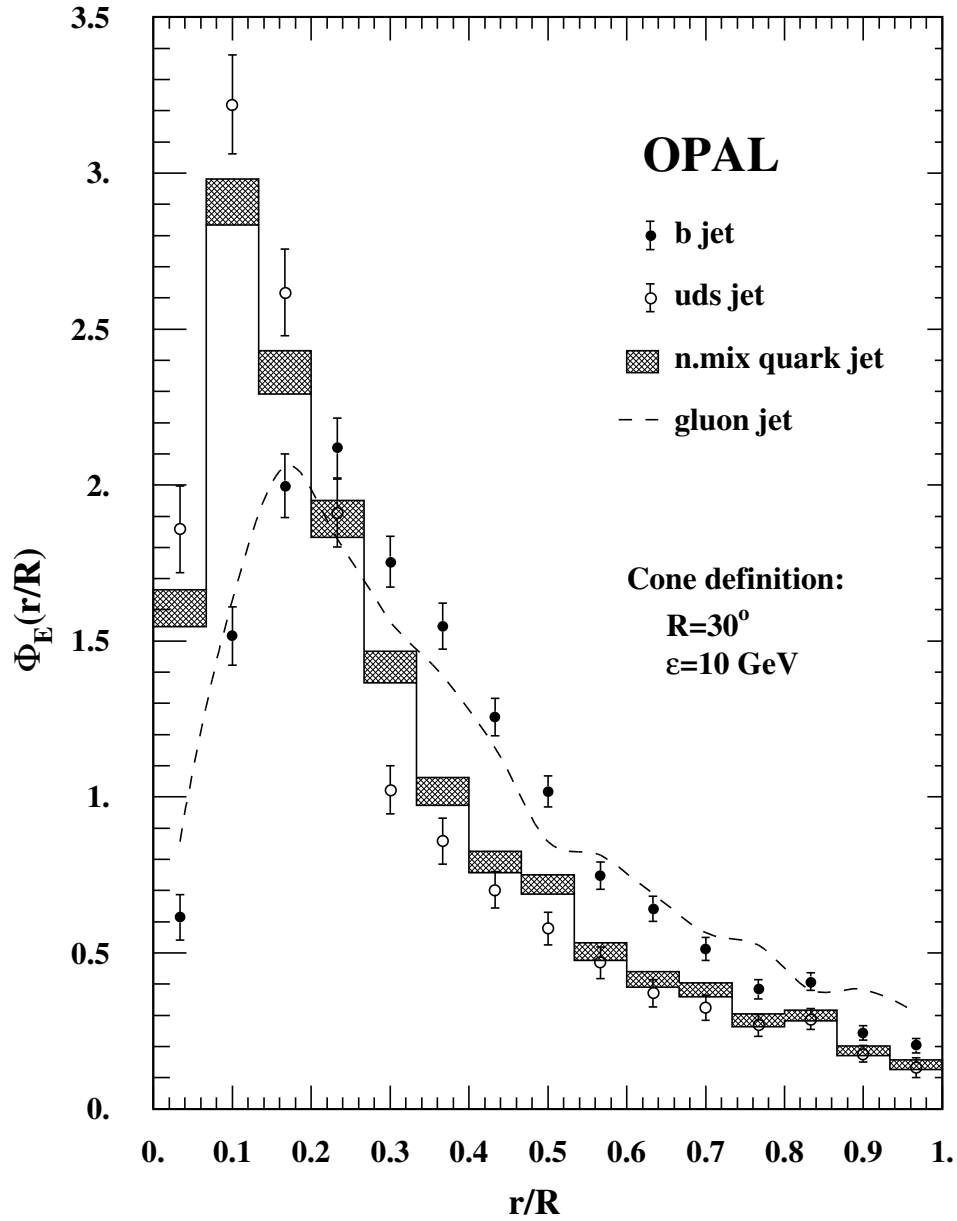
Figure 25: Comparison of b jet, uds jet, normal-mixture quark jet and gluon jet data for the differential energy profile, defined using the cone jet finder. The errors show the experimental statistical uncertainties.
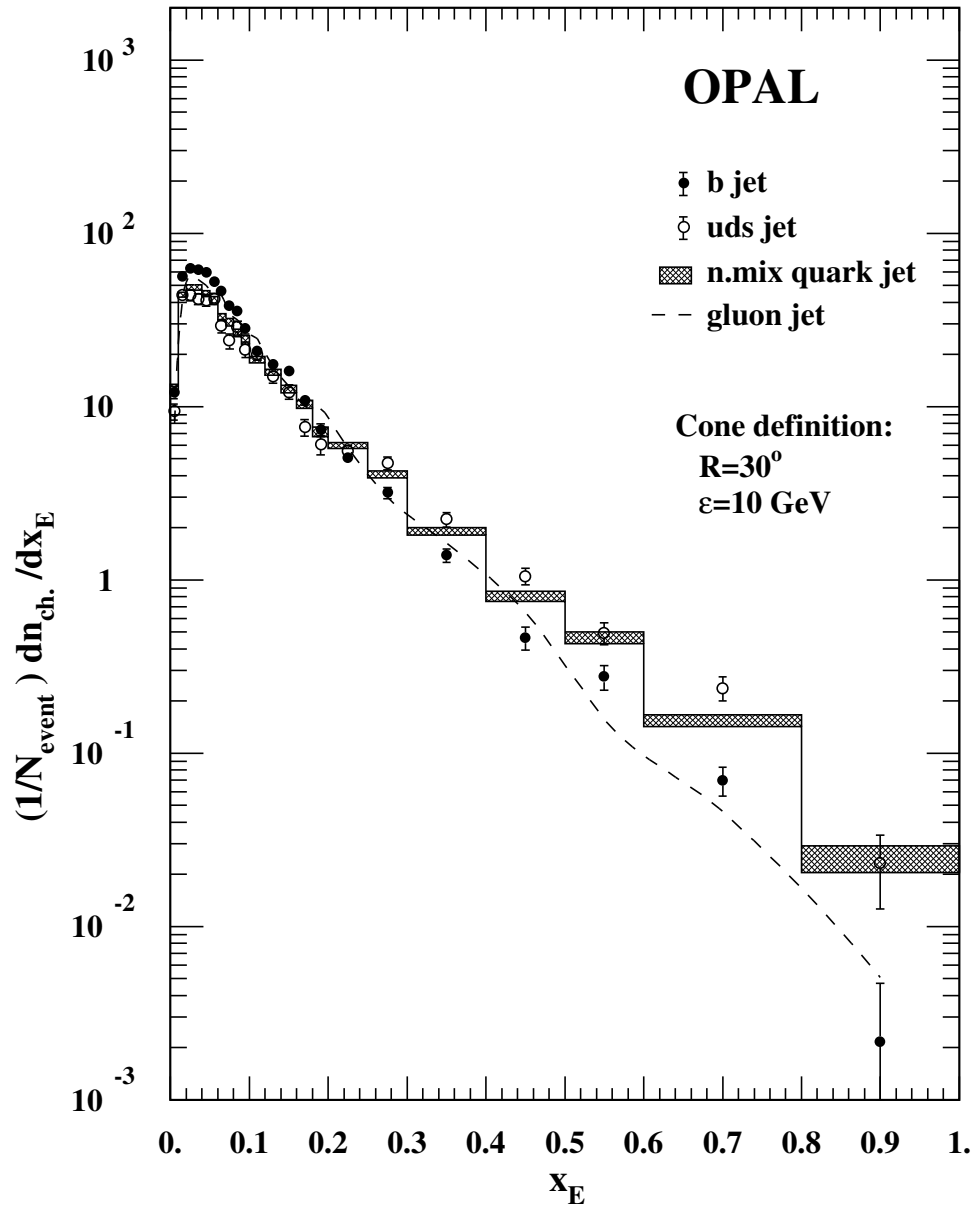
Figure 26: Comparison of b jet, uds jet, normal-mixture quark jet and gluon jet data for the charged particle fragmentation function, defined using the cone jet finder. The errors show the experimental statistical uncertainties.